The Company of **Biologists**

RESEARCH ARTICLE

High P_{CO_2} does not alter the thermal plasticity of developing Pacific herring embryos during a marine heatwave

Christopher S. Murray* and Terrie Klinger

ABSTRACT

Forage fish tend to respond strongly to environmental variability and therefore may be particularly sensitive to marine climate stressors. We used controlled laboratory experiments to assess the vulnerability of Pacific herring (*Clupea pallasii*) embryos to the combined effects of high partial pressure of carbon dioxide (P_{CO_2}) and a simulated marine heatwave. The two P_{CO_2} treatments reflected current conditions (∼550 µatm) and a future extreme level (∼2300 µatm). The dynamics of the heatwave (i.e. rate of onset: ∼0.85°C day^{-1}; maximum intensity: +4.4°C) were modeled from the most extreme events detected by a long-term regional temperature dataset. Simultaneous exposure to these potential stressors did not affect embryo survival. However, the heatwave did elicit significant metabolic effects that included higher rates of routine metabolism (Q_{10}=1.15–1.72), growth (Q_{10}=1.87), rate of development to hatch (Q_{10}=3.01) and yolk consumption (Q_{10}=3.21), as well as a significant reduction in production efficiency (−10.8%) and a three-fold increase in the rate of developmental anomalies. By contrast, high P_{CO_2} conditions produced comparatively small effects on vital rates, including a significant increase in time to hatch (+0.88 days) and a reduction in routine metabolic rate (−6.3%) under the ambient temperature regime only. We found no evidence that high P_{CO_2} increased routine metabolic rate at either temperature. These results indicate that Pacific herring embryos possess sufficient physiological plasticity to cope with extreme seawater acidification under optimal and heatwave temperature conditions, although lingering metabolic inefficiencies induced by the heatwave may lead to important carryover effects in later life stages.

KEY WORDS: Ocean acidification, Extreme climatic events, *Clupea pallasii*, Early life history, Metabolic rates, Embryogenesis, Survival

INTRODUCTION

Extreme climatic events, in which environmental conditions rapidly shift beyond predictable variability, pose an immediate threat to ecological communities (Frölicher et al., 2018; Wernberg et al., 2013; Wetz and Yoskowitz, 2013). Phenotypic plasticity may allow individual organisms to withstand periods of extreme stress by adjusting their phenotype through changes in gene expression or function to match the new environment (Fox et al., 2019; Seebacher

School of Marine and Environmental Affairs and Washington Ocean Acidification Center, University of Washington, 3707 Brooklyn Ave NE, Seattle, WA 98105, USA.

*Author for correspondence (csm187@uw.edu)

C.S.M., 0000-0001-8504-9054; T.K., 0000-0003-2430-0246

et al., 2015). However, the capacity for phenotypic plasticity is inherently limited, and thus successful acclimatization will depend on the specific attributes of the extreme event (i.e. the rate of onset, intensity and duration). This situation is complicated further by the fact that plasticity can vary with ontogeny such that specific life stages face a heightened vulnerability to potential stressors (Burggren, 2018). For example, marine fish display a range of plastic responses in behavior, morphology, phenology and physiology that enable species and populations to persist across large spatial and temporal environmental gradients (Jonsson and Jonsson, 2019). However, fish embryos lack the robust homeostatic capacity that is enabled by mature organ systems and must rely largely on molecular mechanisms rather than behavioral plasticity to counter stressful conditions (Dahlke et al., 2020b; Melzner et al., 2009). Indeed, the early life stages of many fish taxa constitute a critical sensitivity bottleneck in the face of emerging climate change (Baumann, 2019; Esbaugh, 2018; Pörtner and Peck, 2010).

Given that the thermal biology of fish embryos has been studied for decades, there are clear expectations regarding how physiological processes will respond to warming. For example, we know that embryos of temperate fish species have a very limited capacity to regulate metabolic rate against acute temperature change [across-species mean temperature coefficient (Q_{10})≈3.0] and consequently embryos exhibit roughly half the thermal tolerance range compared with juveniles and non-spawning adults of the same species (Rombough, 2011, 1997). By contrast, the extent to which embryonic metabolism is affected by elevated partial pressures of carbon dioxide (P_{CO_2}) consistent with near-future ocean acidification (OA) is less understood. Embryos with underdeveloped gills and circulatory systems rely predominantly on intracellular mechanisms of pH control (Brauner et al., 2019; Mölich and Heisler, 2005). Acid–base perturbations can be responded to through the increased expression of membrane-bound ion pumps, transporters and gas channels (Brauner et al., 2019; Talbot et al., 2015; Tseng et al., 2013). Acidification also triggers the upregulation of stress and repair genes, including heat shock proteins and enzymes involved in antioxidant pathways (Tiedke et al., 2013). Maintaining these functions under elevated P_{CO_2} can be energetically costly and observations of isolated fish tissues have shown that acidification triggers higher metabolic rates (Heuer and Grosell, 2016; Kreiss et al., 2015). If embryos allocate their fixed energetic reserves in a compensatory manner, then the redirection of energy towards acid–base homeostasis should come at the expense of critical growth and development (Rombough, 1994). Furthermore, acidification could limit thermal acclimation because the additional energetic costs of acid–base regulation could reduce the pool of energy available to support higher metabolic rates during acute warming (Pörtner, 2008).

To date, very few studies have performed respiratory measurements on fish embryos to test for metabolic shifts under

List of symbols and abbreviations

A	assimilation
A_T	total alkalinity
CI	confidence interval
CRM	certified reference material
ddpf	degree-days post-fertilization
DIC	dissolved inorganic carbon
dpf	days post-fertilization
dph	days post-hatch
E	excretion
hpf	hours post-fertilization
LMM	linear mixed model
$\dot{M}_{O_2}$	oxygen consumption rate
NERRS	National Estuarine Research Reserve System
OA	ocean acidification
P	production
PCA	principal components analysis
P_{CO_2}	partial pressure of carbon dioxide
pH_{NIST}	pH on the National Institute of Standards and Technology scale
pH_T	pH on the total scale
Q_{10}	temperature coefficient
R	respiration
RMR	routine metabolic rate

elevated P_{CO_2} conditions consistent with OA. Atlantic cod (*Gadus morhua*) and polar cod (*Boreogadus saida*) showed an ~10% increase in respiration rates when exposed to 1100 µatm P_{CO_2} across most of the respective temperature ranges, except for extreme high temperatures, where the effect was reversed and elevated P_{CO_2} induced a 10–20% reduction to rates of oxygen consumption (Dahlke et al., 2018, 2017). The authors hypothesized that this metabolic response to combined stressors was the result of reduced mitochondrial capacity to form ATP. In all cases, elevated P_{CO_2} acted to reduce the size of newly hatched cod by 10–13%. By contrast, elevated P_{CO_2} had no effect on embryonic metabolism or growth across relevant temperature ranges in the Antarctic dragonfish (*Gymnodraco acuticeps*; Flynn et al., 2015), Atlantic herring (*Clupea harengus*; Leo et al., 2018) and Atlantic silverside (*Menidia menidia*; Murray and Baumann, 2018; Schwemmer et al., 2020). Embryos of the ocellated wrasse (*Symphodus ocellatus*) that were transplanted into a high P_{CO_2} environment adjacent to a volcanic CO_2 seep showed an ~50% increase in respiration, whereas embryos sourced from a population endemic to the CO_2 seeps showed no effect (Cattano et al., 2016). Thus, local adaptation to prevailing P_{CO_2} conditions or multigenerational plasticity could help shape CO_2 reaction norms among offspring (Murray et al., 2014). Together, these studies suggest that elevated levels of P_{CO_2} consistent with future acidification (1000–2000 µatm) will produce neutral to perhaps moderate (<±20%) changes to the metabolic rates of fish embryos. Yet, the paucity of studies and species tested to date limits the ability to predict responses in unexamined taxa, particularly when combined with extreme temperature variability.

In the Pacific Northwest (USA), marine ecosystems are under threat from the major climate-associated stressors, including OA and extreme heatwave events (Mauger et al., 2015). The Salish Sea ecosystem is particularly vulnerable to OA owing to a confluence of anthropogenic and natural factors that already cause seasonal P_{CO_2} levels to regularly exceed those shown to be stressful for some marine ectotherms (Evans et al., 2019; Fassbender et al., 2018; Feely et al., 2010), and these will worsen in the future (Pacella et al.,

2018). At the same time, the region has recently experienced a series of marine heatwave events, defined as prolonged periods of anomalously warm ocean temperatures that are quantitatively distinct in time and space (Hobday et al., 2016). The North Pacific marine heatwave of 2014–2016 was among the most extreme events on record, during which positive temperature anomalies of 3–6°C persisted for months at a time over much of the northeast Pacific (Bond et al., 2015; Di Lorenzo and Mantua, 2016; Gentemann et al., 2017). The ecological toll of this event was considerable as effects were felt at all trophic levels (Fisher et al., 2020; Piatt et al., 2020; von Biela et al., 2019). Nearshore habitats face the compounding threat of intense atmospheric heatwaves that can rapidly warm shallow systems over the course of hours to days, with lethal consequences for nearshore organisms (Schlegel et al., 2017; Thomsen et al., 2019). For most coastal regions, the frequency of acute nearshore heatwaves remains largely unquantified and the potential for interactions with large-scale marine heatwaves is complex and poorly described, which limits our ability to anticipate how severe these events might become in the immediate future (Schlegel et al., 2017).

Forage fish dominate the mid-trophic levels of many coastal marine ecosystems and serve as a critical conduit of biological production from lower trophic levels to higher order predators (Pikitch et al., 2012). The life history characteristics of many forage fishes lend to 'boom or bust' population dynamics because recruitment processes are heavily influenced by environmental variability (Szuwalski et al., 2019; Szuwalski and Hilborn, 2015). Consequently, the future viability of forage fish stocks is complicated by marine climate change (Merino et al., 2010; Shannon et al., 2009). The Pacific herring (*Clupea pallasii*) occupies a central position in the Salish Sea food web, and all life stages serve as important prey items for a multitude of marine taxa, including sea birds, mammals, and commercially important fish and invertebrates (Penttila, 2007). Despite reduced fishing pressure and intensive conservation efforts, the spawning stock biomass of several Salish Sea herring populations has declined in recent decades (Sandell et al., 2019; Siple and Francis, 2016; Siple et al., 2017). Understanding how extreme environmental variability will influence herring recruitment processes is a question of ecological and socio-economic importance.

Pacific herring reproduce in shallow nearshore environments where adults adhere fertilized embryos to submerged vegetation (Penttila, 2007; Shelton et al., 2014). In the Salish Sea, these nearshore systems have been modified by human activities (Penttila, 2007) and are exposed to episodic events of low seawater pH associated with sharp fluctuations in P_{CO_2} (Evans et al., 2019; Pacella et al., 2018). Spawning phenology is tightly correlated with photoperiod (Petrou et al., 2021), and 20 of the 21 spawning populations found in the southern Salish Sea reproduce from January to April, when water temperatures are generally below 11°C, with the exception of the Cherry Point stock, which reaches peak reproductive activity in late May (Hay, 1985; Sandell et al., 2019). Decades of empirical research have demonstrated that the viability of Pacific herring embryos is maximized between 8 and 10°C and quickly declines with increasing temperature (Alderdice and Hourston, 1985; Alderdice and Velsen, 1971; Dinnel et al., 2010). In the Salish Sea, nearshore heatwaves occur during all seasons (see Supplementary Materials and Methods) and severe acidification events frequently occur during winter and spring (Evans et al., 2019). The simultaneous emergence of these potential stressors shortly after a spawning event could compromise the viability of entire cohorts of newly fertilized embryos.

Clupeid offspring have been shown to be sensitive to the combined effects of elevated P_{CO_2} and temperature through changes in survival and development (Franke and Clemmesen, 2011; Frommel et al., 2014; Leo et al., 2018; Sswat et al., 2018; Villalobos et al., 2020). Yet, the phenotypic plasticity of Pacific herring embryos exposed to combined climate stressors remains understudied, thereby constituting a serious knowledge gap for this critically important species. Accordingly, we used laboratory experiments to test the hypothesis that a heatwave event will reduce embryo survival and metabolic efficiency and that high P_{CO_2} conditions will aggravate physiological effects by (1) increasing the energetic requirements of acid–base regulation while (2) simultaneously limiting the pool of energy that is available for effective thermal acclimation.

MATERIALS AND METHODS
Collection and description of spawning adults
Animal care and experimental procedures followed the guidelines set forth by the Animal Care Office of Western Washington University (protocol no. 20-002). Wild *Clupea pallasii* Valenciennes in Cuvier and Valenciennes 1847 that were ripe for spawning were collected from Semiahmoo Bay, WA, USA, on 19 February 2020 by the Washington Department of Fish and Wildlife. The Semiahmoo Bay population is a winter-spawning stock that reproduces during February through early March (Sandell et al., 2019). Despite considerable spatial overlap with the spring-spawning Cherry Point stock, the two populations remain genetically isolated as a result of differing phenological patterns (Petrou et al., 2021; Small et al., 2005). The Semiahmoo Bay population does retain considerable genetic exchange with the other winter-spawning stocks from the Salish Sea (Small et al., 2005). Gonads were dissected from nine females and three males and were stored in glass dishes covered with moist paper towels at 4.5°C for 48 h (Dinnel et al., 2010). The mean (±s.d.) total length, wet mass and gonadic–somatic index of female and male spawners was 18.4±1.0 and 19.7±1.3 cm, 51.9±7.3 and 59.6±13.9 g, and 19.5±3.0 and 17.2±1.7%, respectively.

Criteria for treatment P_{CO_2} and temperature conditions
The experiment was conducted at Western Washington University's Shannon Point Marine Center (Anacortes, WA, USA) using 16 purpose-built experimental flow-through units. Embryos were reared under two P_{CO_2} levels [low P_{CO_2}: ~550 µatm, pH on the total scale (pH$_T$) 7.88; elevated P_{CO_2}: ~2300 µatm, pH$_T$ 7.30] crossed with two temperature regimes (ambient and heatwave). The low P_{CO_2} treatment is representative of surface seawater conditions for the Salish Sea during late winter (Fassbender et al., 2018), whereas the high P_{CO_2} treatment reflects maximum of end-of-century P_{CO_2} predicted for the coastal ecosystems of the Pacific Northwest (Evans et al., 2019; Pacella et al., 2018). The ambient temperature treatment fluctuated with the natural conditions (average: 8.8±0.3°C, range: 8.1–10.4°C; Fig. 1) at the laboratory's seawater source (Guemes Channel, 48°30′34.5″N 122°41′04.5″W), which is near the optimal temperature for embryonic development of Salish Sea Pacific herring (Alderdice and Velsen, 1971; Dinnel et al., 2010). All embryos were reared at ambient temperature conditions until ~3.5 days post-fertilization (dpf) or approximately one-quarter of the embryonic duration for *C. pallasii* at ~8.8°C (Kawakami et al., 2011). Heatwave conditions were initiated 88 h post-fertilization (hpf) in half of the replicate tanks per P_{CO_2} level (treatment N=4). Temperatures were increased by ~0.85°C day^{-1} for five consecutive days to achieve a heatwave

condition of +4.4°C above ambient (~8.8°C to ~13.2°C), which was maintained for the duration of the experiment (Fig. 1).

Heatwave characteristics (i.e. rate of onset, duration and maximum intensity) were determined by analyzing a 19-year temperature dataset from the nearby NERRS Ploeg Channel monitoring station in Padilla Bay, WA [48°33′22.8″N 122°31′51.2″W; http://www.nerrsdata.org (accessed 2 November 2019)]. The station monitors a channel that drains a network of eelgrass beds and tidal flats and thus conditions are broadly representative of herring spawning habitat in the Salish Sea (Bulthuis, 2013). The R package heatwaveR (Schlegel and Smit, 2018) was used to identify heatwaves in the time series based on selection criteria of daily mean temperatures exceeding the 90th percentile of the long-term seasonal climatology for a minimum of five consecutive days (Hobday et al., 2016). The experimental heatwave treatment was based on the average characteristics of the top five heatwave events on record corresponding to a category 2 heatwave as defined by Hobday et al. (2018). See Supplementary Materials and Methods for complete details. The viability of Pacific herring embryos begins to decline from optimal as temperature exceeds 10.5°C and embryonic viability rapidly declines when incubation conditions climb above 13°C (Fig. S1; Alderdice and Velsen, 1971; Dinnel et al., 2010). Thus, the maximum temperature of the simulated heatwave event may approach critical temperature thresholds where interactive effects with high P_{CO_2} are hypothesized to emerge (Lefevre, 2016; Pörtner, 2010).

Experimental system
The 16 experimental units were each composed of an elevated 40-liter mixing tank and a 12-liter main rearing tank. The mixing tank received a continuous supply (~1 l min^{-1}) of filtered (to 1 µm) seawater (salinity ~32 ppt) with a stable pH$_T$ of ~7.66. To achieve high P_{CO_2} conditions, the mixing tank continuously received standardized doses of CO_2 gas (99% CO_2, AirGas) delivered by an eight-channel peristaltic pump (Masterfelx L/S, Cole-Parmer). CO_2 was injected directly into the intake of a submersible pump with magnetically driven impellers to promote an even dissolution. Low P_{CO_2} conditions were achieved by stripping CO_2 from compressed air (CO_2 adsorber, Twin Tower Engineering), which was then bubbled directly into mixing tanks to purge dissolved inorganic carbon (DIC) from seawater. All mixing tanks were continuously bubbled with compressed laboratory air to maintain a dissolved oxygen partial pressure (P_{O_2})>85% air saturation. Heatwave temperatures were controlled by Elitech STC-1000 controllers that powered three 100 W heaters (Aqueon) per unit. During heatwave onset, temperature set points were increased by 0.5°C every 12 h. Small aquarium pumps were positioned in the main rearing tanks to ensure even heating.

Experimental embryos were housed in customized 0.5-liter polyethylene rearing baskets fitted with 300-µm mesh bottoms. Baskets were floated in the main rearing tank. Treated seawater from the mixing tanks was gravity-fed directly into baskets at standardized rates (~0.5 ml s^{-1}). The temperatures of main rearing tanks were recorded automatically every 30 min starting at 3 dpf (HOBO® Pendant Temp, Onset). Embryo baskets were measured for pH and temperature every ~12 h by a handheld pH meter (Orion Star A221 meter, 9107BNMD pH triode, Thermo Fisher Scientific) which was calibrated daily with three-point NIST buffers (Fisher Chemical). The pH electrode was cleaned daily in 0.1 mol l^{-1} HCl and the reference solution was completely exchanged every 5 days. Measured pH$_{NIST}$ values were converted to pH$_T$ via a probe-specific conversion formula (see Supplementary Materials and Methods). Dissolved oxygen levels were

3
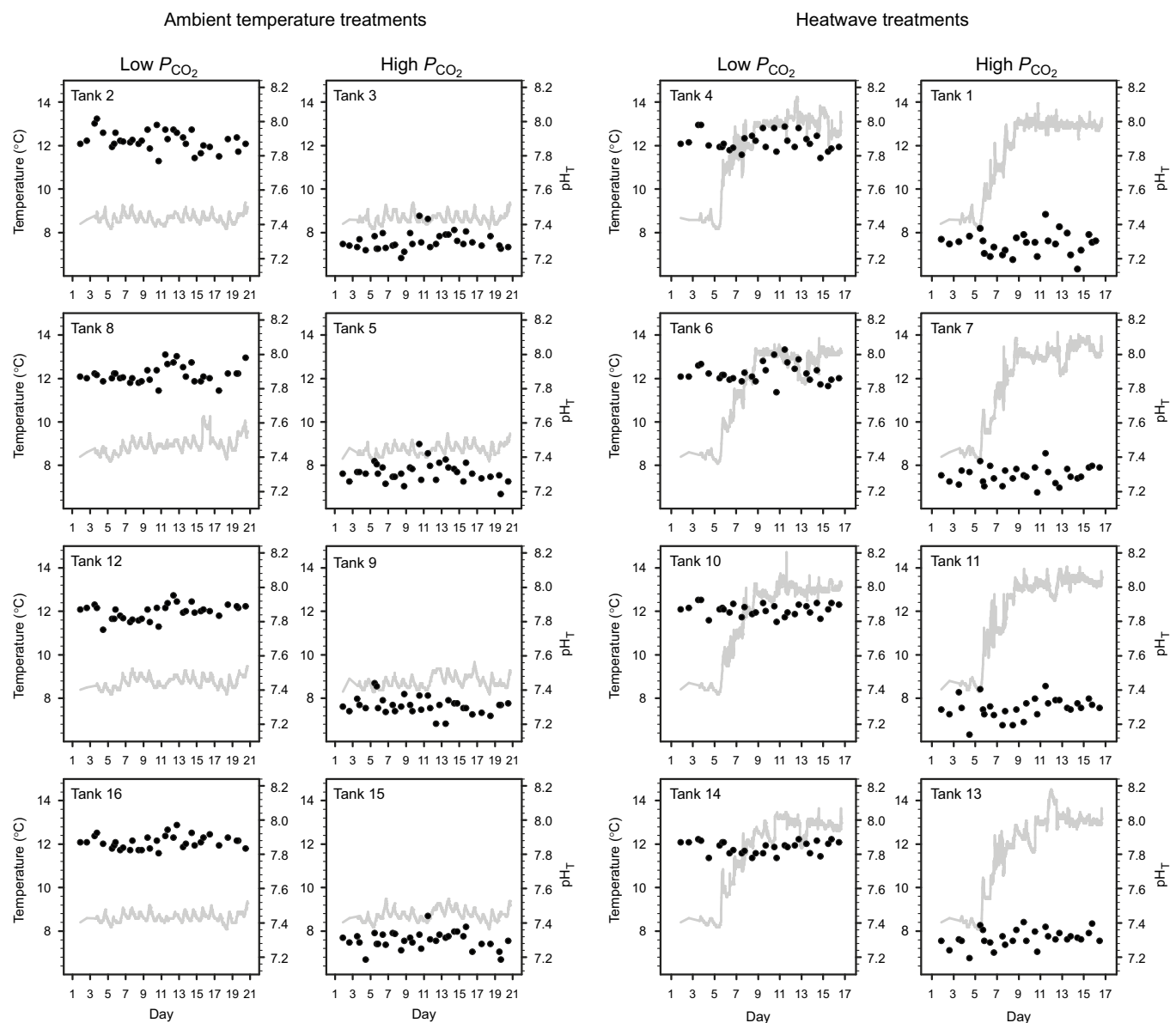
Fig. 1. Treatment conditions by replicate tank. Continuous temperature measurements (gray lines) and daily spot-checks of pH on the total scale (pH_T ; black circles) in 16 replicate tanks. Note that the experimental trials were terminated at the end of the hatching period (heatwave: 17 dpf; ambient temperature 21 dpf).

checked daily with a handheld meter (YSI Model 55) that was calibrated daily using 100% water-saturated air. Embryos were exposed to dim light over a natural light cycle (11 h:13 h light:dark). Experimental pH and temperature conditions are summarized in Fig. 1.

Carbonate chemistry
Discrete seawater samples (25 ml) were taken every third day from each replicate tank (n=5 samples per heatwave replicate; n=6 samples per ambient replicate) for direct measurements of pH_T and DIC following methods described by Love et al. (2017). Temperature, pH_{NIST} and salinity were recorded at the time of sampling using the handheld electrode. The samples were filtered to 0.6 µm, poisoned with 10 µl of saturated mercuric chloride solution and stored in 25-ml scintillation vials at 2°C. Restricted access to laboratory facilities during the spring of 2020 led to an unplanned and prolonged delay in sample processing (~4 months) during which significant off-gassing of dissolved CO_2 from high

P_{CO_2} samples occurred. Therefore, additional steps were required to estimate carbonate chemistry parameters.

A DIC analyzer (Apollo SciTech AS-C3) was calibrated by developing a standard curve based on five measurements of different volumes (0.5–1.5 ml) of certified reference material (CRM; batch no. 169; Andrew Dickson, University of California San Diego, Scripps Institution of Oceanography, https://www.nodc. noaa.gov/ocads/oceans/Dickson_CRM/batches.html). To measure DIC, samples were warmed to room temperature and the analyzer extracted a minimum of three 1-ml measurements per sample, consisting of a blank followed by at least two consecutive duplicate measurements within 2 µmol l^{-1} . DIC was converted to µmol kg^{-1} using the sample density based on measurement room temperature and sample salinity. Seawater samples were analyzed concurrently for pH_T using a diode array spectrophotometer (Agilent 8453A UV-VIS). Seawater was injected by syringe into a 5-cm jacketed cuvette that was maintained at room temperature via circulated water from a thermostat bath. After the cuvette was loaded into position and the

spectrophotometer was blanked, two 30-μl aliquots of m-cresol dye (lot no. MKBR3556V) were injected into the cuvette to generate 'two-shot' duplicate measurements of absorbance at three wavelengths (730, 578 and 434 nm). Calculations for pH_T were based on absorbance ratios by following Dickson et al. (2007) and included a lot-specific dye correction.

CO_2 off-gassing meant that measured DIC and pH_T could not be directly used to estimate treatment P_{CO_2} conditions. However, the measurements were sufficient for estimating *in situ* total alkalinity (A_T, μmol kg^{-1}) at the time of sampling given that the A_T of poisoned samples is unaffected by gas exchange and will closely reflect conditions at the time of sampling in the absence of biological activity (Dickson et al., 2007). Sample A_T was calculated using the R package seacarb (https://cran.r-project.org/package=seacarb) based on direct measurements of salinity, DIC, pH_T, typical nutrient levels for the seawater source (total P: 2.2 μmol kg^{-1}; total Si: 2 μmol kg^{-1}), and the room temperature during DIC and pH_T measurements. Equilibrium constants for the dissociation of carbonic acid in seawater (K1 and K2) followed Mehrbach et al. (1973) refitted by Dickson and Millero (1987) and the constant for KHSO$_4$ from Dickson (1990). This method was able to consistently reconstruct the A_T of Dickson CRMs within ±1% and derived A_T values closely matched a regional salinity and alkalinity relationship (+2% on average; Fassbender et al., 2016).

The remaining *in situ* seawater chemistry parameters of P_{CO_2}, DIC and carbonate and bicarbonate ion concentrations (CO_3^{-2}, HCO_3^{-}; μmol kg^{-1}) were calculated in seacarb using derived A_T, typical nutrient levels, and the *in situ* salinity, temperature and pH_{NIST} levels that were recorded at the time of sampling during the experiment. To reduce the error associated with seawater pH measurements calibrated on the NIST scale (Dickson et al., 2015), an extensive cross-calibration between the handheld electrode and the diode array spectrophotometer was conducted to produce a robust probe-specific linear relationship to convert pH_{NIST} values to pH_T ($N=36$, $R^2=0.997$; see Supplementary Materials and Methods for complete details):

$$pH_T = 0.91344 \times pH_{NIST} + 0.59905. \quad (1)$$

All seacarb calculations used converted pH_T values. A summary of treatment carbon chemistry is listed in Table 1.

Fertilization protocols
Embryos were fertilized on 21 February 2020 following established protocols (Dinnel et al., 2010). Gonads were slowly warmed in a walk-in environmental chamber to the fertilization temperature (8.5°C). Four large plastic dishes (two per P_{CO_2} treatment) were lined with 300-μm nylon mesh screening and then were filled with 750 ml of filtered and autoclaved seawater (salinity 32) that was adjusted to 550 or 2300 μatm P_{CO_2}. Five 1-cm^2 sections of teste were sampled from each male and were eviscerated together on a 300 μm screen and the milt was filtered into a glass beaker filled with 1 liter

of clean seawater. The milt solution was mixed and 250 ml was poured into each spawning dish. Small groups of healthy eggs from a single female were then scooped sequentially into the spawning dishes such that eggs were equally but randomly distributed to the four dishes. This process continued with each female until the spawning screens were largely covered with a single layer of eggs. Gametes were left to soak for 1 h after which the screens were rinsed with clean seawater to remove milt and unattached eggs. Adhered embryos were disinfected for 10 min in a 100 ppm Ovadine–seawater solution (Western Chemical). Screens were haphazardly cut into small sections and hung within the floating embryo baskets in each of the four replicate tanks per treatment.

Sampling design and response variables
Fertilization success
Embryos were randomly subsampled ($n>20$) at 46 hpf from each replicate and photographed using a digital camera (MC170 HD, Leica) mounted on a dissection microscope (SZ40 stereomicroscope, Olympus) to produce calibrated digital images (Leica Application Suite). Fertilization status was determined by the presence or absence of a raised fertilization membrane (Dinnel et al., 2010). Fertilization success was quantified as the ratio of fertilized eggs to the total number of eggs visible in the frame.

Embryo survival
At exactly 2 dpf, 100 fertilized embryos were randomly selected and distributed to a new rearing basket to quantify survival rates to hatching. The remainder of the embryos were maintained in a separate basket for measurements of developmental and metabolic rates. An accident compromised an embryo survival replicate (tank 1; heatwave×high P_{CO_2}) and it was removed from the experiment. Baskets were inspected at noon of each day and newly hatched larvae were counted, removed and evaluated for obvious developmental anomalies including hatchlings that exhibited notochord twists, shortenings and curvatures that exceeded 90 deg as well as edemas present in the yolk sac and underdeveloped jaws (Dinnel et al., 2010; Hershberger et al., 2005; Purcell et al., 1990). See Fig. S2 for examples of anomalies. The experimental trials were terminated after three consecutive days of no hatching within each temperature group, which occurred at 17 and 21 dpf under heatwave and ambient temperatures, respectively. The remaining embryos were counted and inspected for developmental status and all unhatched individuals were confirmed to be dead. Total hatch (%) was calculated as the number of hatched larvae (including anomalies) divided by the number of embryos at experiment initiation ($n=100$). Anomaly rate (%) was calculated as the number of anomalous larvae per 100 initial embryos. Hatching success (%) was calculated as the total number of hatched embryos minus the number of anomalous larvae divided by 100 initial embryos. Time to peak hatch was defined as the dpf to 50 cumulative hatchlings. A developmental rate (% day^{-1}) was calculated for each replicate as 100% divided by dpf to peak hatch.

Table 1. Carbon chemistry

Treatment	pH_T	P_{CO_2}	A_T	DIC	HCO_3^{-}	CO_3^{-2}
Ambient, low CO$_2$	7.89±0.05	554±75	2119±29	2020±35	1913±37	81±8.9
Ambient, high CO$_2$	7.30±0.04	2338±216	2117±30	2191±34	2060±30	22.1±1.9
Heatwave, low CO$_2$	7.89±0.04	568±61	2114±31	2003±26	1890±25	88.7±9.1
Heatwave, high CO$_2$	7.31±0.04	2325±236	2113±35	2170±27	2047±28	25.8±3.9

Treatment mean (±s.d.) pH on the total scale (pH_T), partial pressure of CO$_2$ (P_{CO_2}, μatm), total alkalinity (A_T, μmol kg^{-1}), dissolved inorganic carbon (DIC, μmol kg^{-1}), bicarbonate (HCO$_3$, μmol kg^{-1}) and carbonate (CO$_3^{-2}$, μmol kg^{-1}) derived from seawater samples that were preserved every 3 days from each replicate during the duration of the experiment (heatwave: $N=5$; ambient: $N=6$).

Metabolic rate

To estimate treatment effects on the routine metabolic rate (RMR) of pre-absorptive and un-anesthetized embryos (Peck and Moyano, 2016), closed respirometry was used to measure the oxygen consumption rates ($\dot{M}_{O_2}$) of groups of embryos from each replicate tank once per day for three consecutive developmental days. Measurements were initiated at 6 dpf on eye-staged embryos (stage F–G; Kawakami et al., 2011) and then were repeated on 7 and 8 dpf. This period coincided with days 2–4 of the onset of the heatwave. Twenty identical respiration vials were prepared for the experiment: 2.15-ml glass vials fitted at the bottom with a single planar trace oxygen sensor spot (PreSens). All vials were enclosed with screw-tight caps and PTFE/silicone/PTFE septa. Respirometry trials were run separately for each temperature treatment on each developmental day such that six total trials were completed. On the day of sampling, groups of 9 or 10 embryos were randomly selected per replicate tank and disinfected in a 100-ppm Ovadine–seawater solution to reduce background microbial respiration. Post-disinfection, embryos were evaluated under a dissection microscope for physical condition and photographed for calibrated measurements of egg surface area (mm^2) and diameter cross-sections from three different axes (mm). Egg volume (V; µl) was estimated from diameter measurements using the ellipsoid formula:

$$V = (4/3)\pi \times r_1 \times r_2 \times r_3, \tag{2}$$

where r is radius. All 9–10 embryos per replicate tank were transferred into a single randomly selected respiration vial filled with UV-sterilized and autoclaved seawater adjusted to treatment temperature and P_{CO_2} levels and a P_{O_2} of ∼100% air saturation. Six respirometry vials were randomly selected to serve as blanks and were filled with air-saturated seawater for a total of 14 vials per trial: 8 embryo vials (one per replicate tank) and 6 blanks. Embryos were allowed to acclimate to vial conditions for 45 min, after which the seawater in the vial was fully exchanged and the vials were sealed. The trials were conducted within a walk-in environmental chamber where the temperature was maintained at the experimental temperature at time of sampling: 8.7–8.8°C for ambient and 11.0, 12.2 and 13.2°C under the heatwave regime at 6, 7 and 8 dpf, respectively. The respirometry vials were submerged in a water bath maintained at the measurement temperature to reduce possible temperature fluctuations when the walk-in door was opened. Trials were conducted in the dark under low red light to minimize disturbance to the embryos.

Oxygen concentrations (µmol l^{-1}) were measured and recorded using a Fibox4 oxygen meter equipped with a PSt3 fiber optic sensor (PreSens) using Presens Measurement Studio (v. 2). The sensor was calibrated prior to each trial with a two-point calibration using air-saturated seawater and a concentrated NaSO$_3$ solution (P_{O_2}=0) adjusted to the trial temperature. After recording initial oxygen concentrations, vials were slowly inverted every 5 min to reduce oxygen stagnation around the embryos. Blank vials were fitted with a small glass bead (4 mm diameter) to promote mixing. Oxygen concentrations were recorded at ∼15 min intervals until levels reached ∼80% air saturation within embryo vials. The duration of trials varied between 71 and 141 min depending on the temperature treatment and age. At the conclusion of the trial, all embryos were recounted and examined for irregularities that would have affected $\dot{M}_{O_2}$ (i.e. mortality or hatching), and none were identified. Respirometry vials were filled and shaken with 90% ethanol for sterilization between trials.

Oxygen consumption data were analyzed in R (v. 4.0.2) using Rstudio (v. 1.3.1). Linear regressions between oxygen concentration and time were fitted for each respirometry vial. Regression residuals were analyzed for outlying values and clear outlying measurements were removed from blank vials only. The correlation of determination (R^2) for all fitted regressions for vials containing embryos was >0.925. Derived slopes were used to calculate rates of individual embryo $\dot{M}_{O_2}$ (nmol O$_2$ h^{-1}) after accounting for the seawater volume of the respirometry vial (total vial volume−total volume of eggs), background oxygen change (calculated as the mean ΔO$_2$ of all blank vials) and the number of embryos per vial. For some trials, the ΔO$_2$ of blank vials was slightly positive, but in all cases blank ΔO$_2$ was less than 8% of ΔO$_2$ in embryo vials. ANOVA indicated that egg surface area was significantly affected by a $P_{CO_2} \times$temperature interaction (F=14.965, P<0.001). To account for the influence of egg size, RMR was standardized to the mean embryo surface area of the vial (nmol O$_2$ h^{-1} mm^{-2}).

Hatch morphometrics

Newly hatched larvae were subsampled (n=12) on the day of peak hatch (heatwave 11 dpf; ambient temperature 14 dpf) from each replicate tank (192 total). Individual larvae were euthanized via an overdose of MS-222, photographed for analysis of morphometric traits, and dried at 60°C for 24 h. Seven size and shape traits were measured in ImageJ (Fig. S2): standard length (tip of the snout to the end of the notochord; nearest 0.01 mm), somatic body area (total tissue surface area minus the yolk sac and finfold, 0.01 mm^2), head width (cranial width immediately posterior to the optic disk; 0.01 mm), mean eye width (eye diameter at widest axis, 0.01 mm), post-yolk body depth (dorsal to ventral tissue height including the gut but minus the finfold immediately posterior to the yolk sac; 0.01 mm), post-vent body depth (tissue height immediately posterior to the anus; 0.01 mm) and yolk sac profile area at hatch (0.01 mm^2). Duplicate dry masses (0.1 mg) were recorded using a micro balance (AT21 Mass Comparator, Mettler Toledo).

After 60 degree-days post-fertilization (ddpf; degree-days=mean incubation temperature×days) at ∼50% development, 10 embryos were sampled from each replicate for measurements of yolk sac surface area at 6 and 7 dpf under heatwave and ambient temperatures, respectively. Replicate mean yolk consumption rates (% day^{-1}) were calculated as the percentage change in yolk sac area from 50% development to hatch divided by the incubation interval in days. Embryo growth rate (mm day^{-1}) was estimated as the replicate mean standard length at hatch divided by age in dpf at hatch. The energy budget of cleidoic fish egg can be balanced as:

$$A = P + R + E, \tag{3}$$

where A represents the total energy assimilated from the yolk (i.e. total consumption), P is tissue production, R is respiration and E is excretion (Rombough, 2011). An estimate of production efficiency (i.e. the ratio of yolk consumed to tissues produced) was derived for each replicate as the log of the ratio of larval body area (production, P, mm^2) to the difference in yolk sac area from 50% development to hatch (assimilation, A, mm^2):

$$\text{Production efficiency} = \log(P \times A^{-1}). \tag{4}$$

Statistical analyses

Statistical analyses were performed in R. Main and interactive effects of P_{CO_2} level and temperature regime were considered

significant at α<0.05. Data are reported as means±1 s.d. unless specified otherwise. Model assumptions were tested using the R package performance (https://CRAN.R-project.org/package=performance). *Post hoc* tests were run using the R package emmeans (https://CRAN.R-project.org/package=emmeans). Plots were produced with ggplot2 (Wickham, 2016). A one-way ANOVA was used to test the effect P_{CO_2} on logit-transformed fertilization success. A two-way ANOVA was used to determine P_{CO_2}×temperature effects on logit-transformed hatching success and time to peak hatch.

A Pearson correlation matrix was constructed to quantify associations between morphometric traits and treatment conditions. A linear dimension reduction was performed on the eight size and shape traits using a principal component analysis (PCA; R package prcomp). The data were centered and scaled prior to PC extraction. Trait correlations, loadings and variance contributions for each PC were calculated in the R package factoextra (https://CRAN.R-project.org/package=factoextra). For each extracted PC, traits with loadings that exceeded ±0.32 were considered practically significant (Tabachnick et al., 2007). Component scores for each PC were assigned to individual larvae. Linear mixed-effect models (LMMs) were constructed to test for significant effects of P_{CO_2}, temperature regime and their interaction (fixed effects) on PC scores and individual morphometric traits. Tank ID was set as a random intercept to account for the common rearing environment of larvae sampled from the same replicate tank. LMMs were run using the R packages lme4 and lmerTest, or nlme to accommodate variance heterogeneity between groups using the weights and varIdent functions (Bates et al., 2014 preprint; Kuznetsova et al., 2017; http://CRAN.R-project.org/package=nlme). Treatment effects on yolk consumption rate, log-transformed embryo growth rate and production efficiency were tested with two-way ANOVAs.

To evaluate treatment effects on embryo RMR, we first used two-way ANOVAs to test the within-temperature effects of P_{CO_2} and embryo age (dpf) on the log-transformed RMR values. Next, two-way ANOVAs tested for significant effects of P_{CO_2} and temperature treatment on log-transformed RMR measurements separately for measurement each day. Temperature coefficients (Q_{10}) for RMR were calculated from embryos at the same developmental stage at 60 ddpf (heatwave: 6 dpf at 11°C; ambient: 7 dpf at 8.8°C) and 70 ddpf (heatwave: 7 dpf at 12.2°C; ambient: 8 dpf at 8.7°C) using the formula:

$$Q_{10} = (RMR_{heatwave}/RMR_{ambient})^{(10/(T_{heatwave}-T_{ambient}))},$$

Q_{10} coefficients provide a standardized calculation of the change in physiological rates to a 10°C increase in temperature. Additional Q_{10} values were calculated for developmental rate, yolk consumption rate and embryo growth rate. For RMR, $T_{heatwave}$ and $T_{ambient}$ were set to the temperatures used during the respective RMR trials. For other traits, the temperature variables were defined as the average temperature experienced by the embryos during the rearing interval over which the trait was evaluated. Q_{10} values were calculated separately for each P_{CO_2} level and on combined P_{CO_2} data. To generate confidence intervals (CIs), Q_{10} calculations were bootstrapped (N=1000) by randomly selecting one replicate value from each temperature treatment and recalculating Q_{10}. Bias-corrected and accelerated 95% CIs were computed using the R function boot.ci (https://CRAN.R-project.org/package=boot) and P-values were calculated from the CIs to quantify significant

differences in Q_{10} values between P_{CO_2} treatments (Altman and Bland, 2011).

RESULTS

Fertilization, hatching and survival

Overall, fertilization success was high (84±7%) and did not significantly vary between P_{CO_2} levels (Table 2). Hatching commenced 10 and 13 dpf in the heatwave and ambient temperature treatments, respectively (Fig. 2). Exposure to the heatwave shortened the average time to peak hatch to 11.0±0.5 dpf compared with 14.5±0.5 dpf under ambient temperatures (ANOVA, P<0.0001; Table 2, Fig. 2). On average, exposure to high P_{CO_2} led to a small but significant delay in hatching by 0.88 days when averaged between temperature treatments (ANOVA, P=0.0007; Fig. 2). No interactive effect between P_{CO_2} and temperature was detected (Table 2).

Total hatch was not affected by P_{CO_2} level, but it was significantly higher in heatwave replicates (90.3±6.9%) compared with the ambient regime (78.4±3.5%) (ANOVA, P=0.001; Table 2, Fig. 3). However, developmental anomalies increased under heatwave conditions by more than three-fold, to 8.9±3.2% (ANOVA, P>0.0001; Table 2, Fig. 3). Mean anomaly rates under heatwave conditions were higher under high (11.3±2.3%) compared with low P_{CO_2} (7.0±2.4%) but the effect was not significant (Table 2). Higher developmental anomalies under the heatwave regime reduced the average hatching success to 81.4±8.9% when pooled across P_{CO_2} treatments, which was not significantly different from ambient replicates (75.6±3.3%) (ANOVA, P=0.0757; Table 2, Fig. 3). Owing to a combination of higher total hatch and slightly lower anomaly rate, hatching success in heatwave×low P_{CO_2} replicates (86.2±7.4%) was, on average, 11 percentage points higher than the heatwave×high P_{CO_2} group (75±6.9%) and both ambient temperature treatments (75–76%; Fig. 3). Despite the difference, the temperature×P_{CO_2} interactive effect was not significant (P=0.0685, Table 2). Interestingly, mean hatching success under heatwave conditions was 19 percentage points higher than the predicted rate for a static exposure to 13.2°C, the maximum intensity of the heatwave (Fig. S2).

Hatch morphometrics

In general, morphometric traits were negatively correlated with the heatwave treatment and were weakly associated with P_{CO_2} level (Table S2, Fig. 4). The first four extracted PCs accounted for 89.8% of the total variance in morphometric traits and were selected for further analysis. PC1 was identified as the body size component and

Table 2. ANOVA results for fertilization success (%), peak hatch (dpf), total hatch (%), anomaly rate (%) and hatching success (%)

Trait	Factor	d.f.	F	P
Fertilization success	P_{CO_2}	1	0.3574	0.5595
Peak hatch	P_{CO_2}	1	21.758	**0.0007**
	Temperature	1	220.958	**<0.0001**
	P_{CO_2}×temperature	1	0.130	0.7251
Total hatch	P_{CO_2}	1	1.6061	0.2312
	Temperature	1	19.5109	**0.0010**
	P_{CO_2}×temperature	1	2.3500	0.1535
Anomaly rate	P_{CO_2}	1	1.4356	0.2560
	Temperature	1	60.5022	**<0.0001**
	P_{CO_2}×temperature	1	2.8524	0.1193
Hatching success	P_{CO_2}	1	2.8725	0.1182
	Temperature	1	3.8461	0.0757
	P_{CO_2}×temperature	1	4.0763	0.0685

Significant P-values indicating treatment effects are denoted in bold.
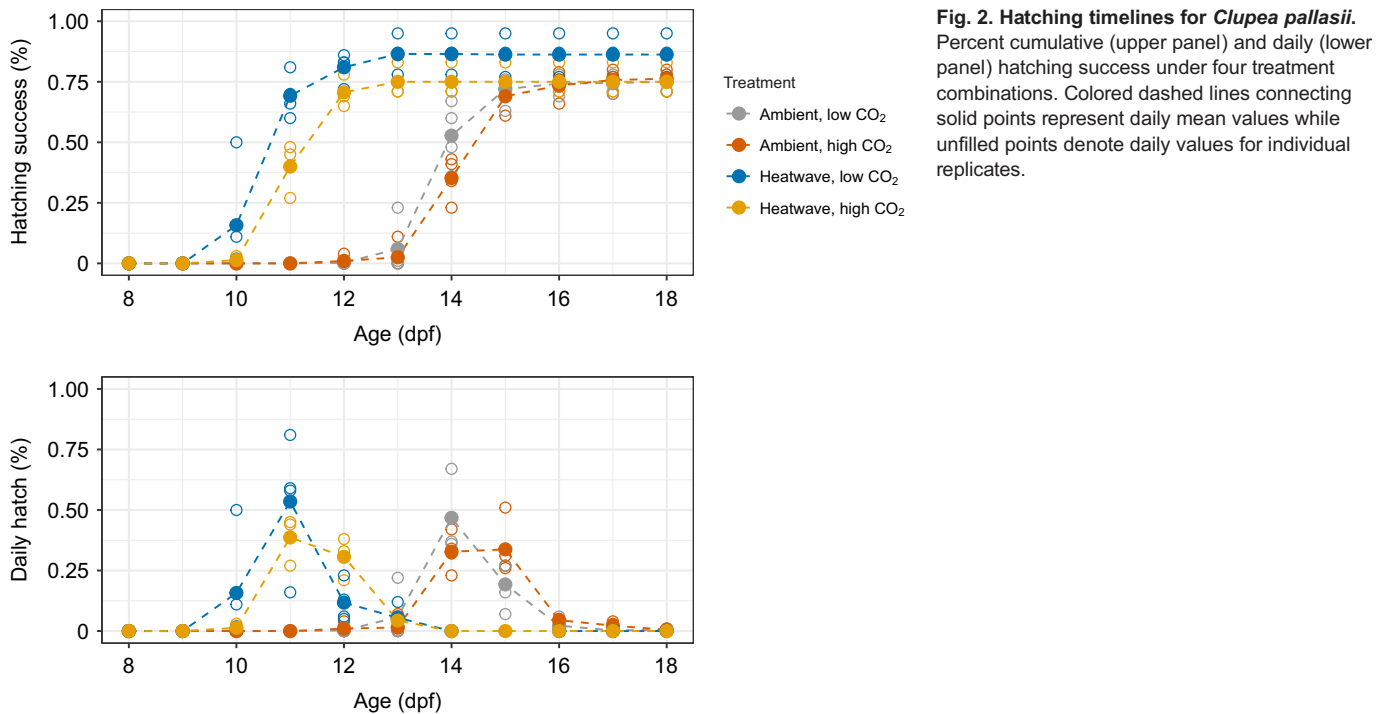
Fig. 2. Hatching timelines for *Clupea pallasii*. Percent cumulative (upper panel) and daily (lower panel) hatching success under four treatment combinations. Colored dashed lines connecting solid points represent daily mean values while unfilled points denote daily values for individual replicates.

accounted for the majority of the variance in size and shape (59%). With the exception of yolk sac area and dry mass, all other traits showed significant positive loadings onto PC1 (Table S2). Newly hatched larvae exposed to heatwave conditions exhibited significantly lower PC1 scores, indicating a general reduction in body size at hatch (LMM, $P<0.001$; Table S3), and individually most morphometric traits were significantly reduced under heatwave conditions (Table S3, Fig. 4). When averaged

across P_{CO_2} treatments, heatwave-exposed hatchlings had a shorter standard length (7.49 ± 0.57 mm) and smaller body area (2.63 ± 0.38 mm^2) relative to the standard length (8.20 ± 0.33 mm) and body area (2.96 ± 0.26 mm^2) of larvae from the ambient treatment. PC1 and thus body size was not significantly affected by P_{CO_2} level (Table S3).

PC2 accounted for 14.7% of the total variance in morphometric traits and largely captured variation associated with yolk sac area
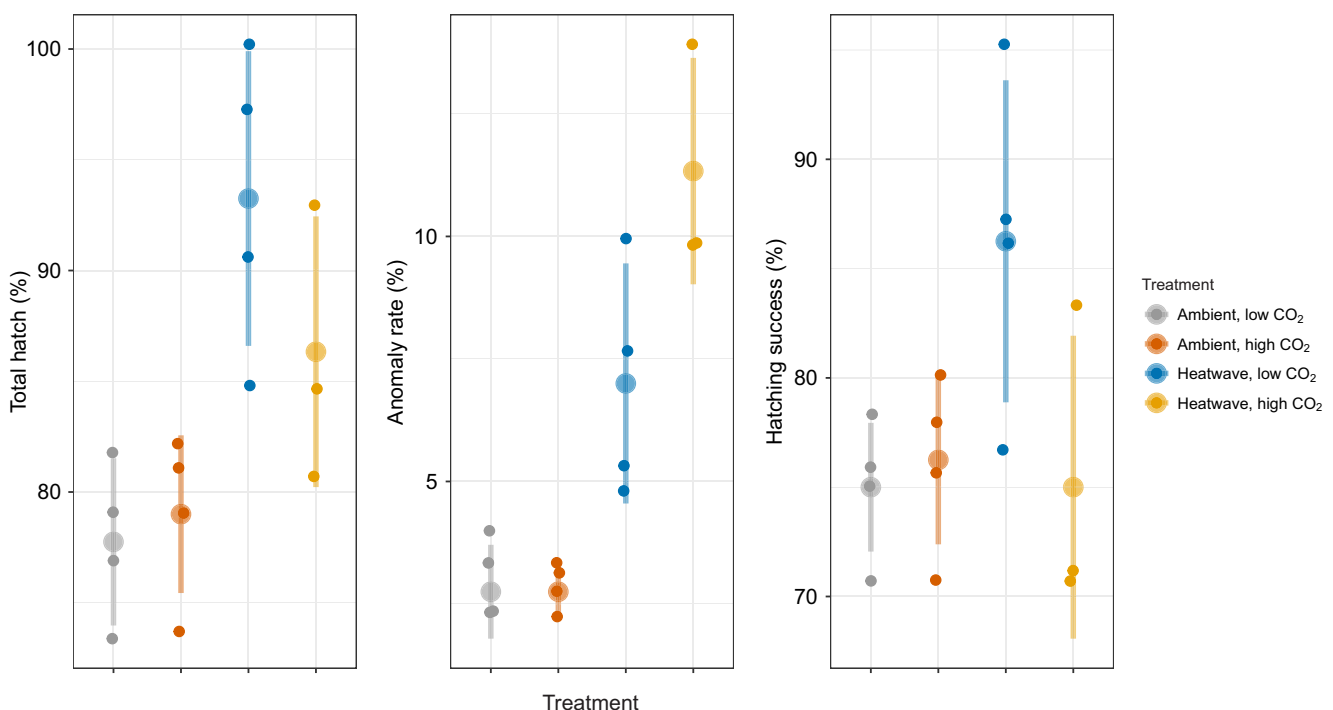
Fig. 3. *Clupea pallasii* total hatch (%), anomaly rate (%) and hatching success (%) under four treatment conditions. Large colored circles with vertical lines represent treatment means±s.d. Small circles show values for individual replicates.
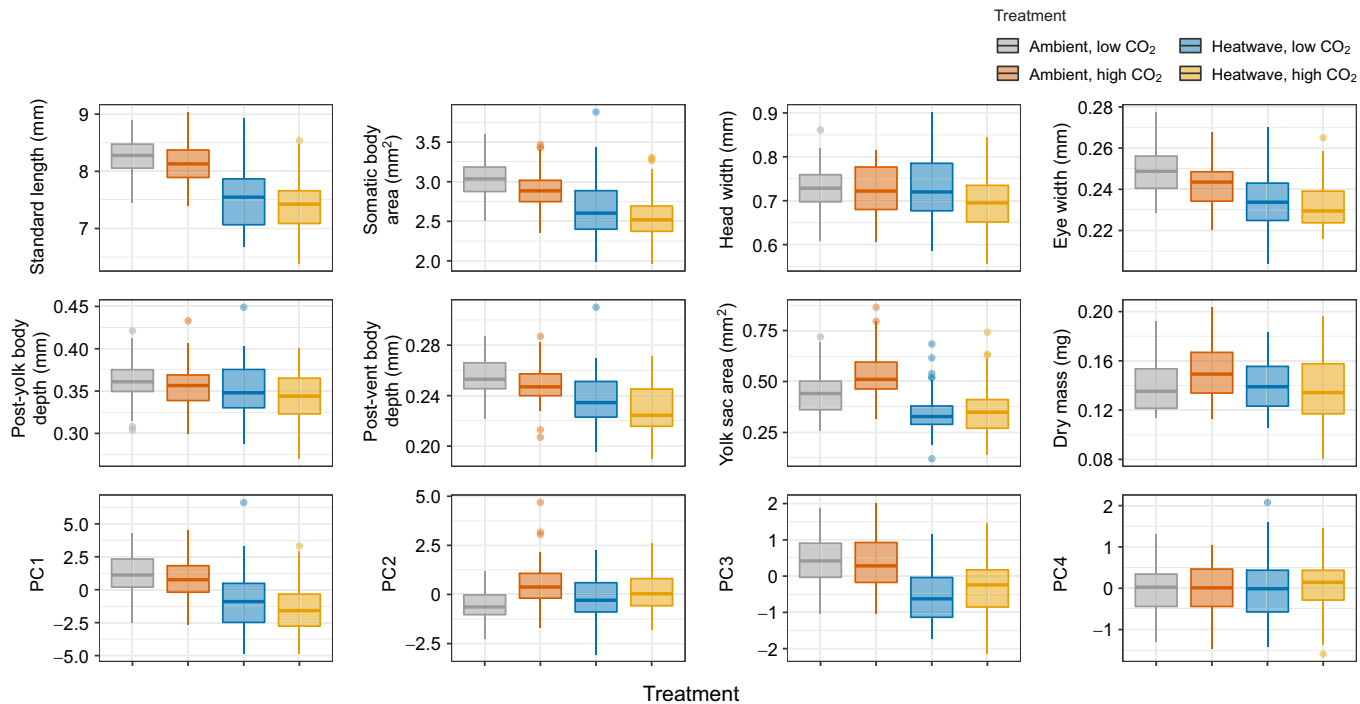
Fig. 4. Morphometric traits and PC scores of *C. pallasii* larvae sampled on the day of peak hatch. Box plots illustrating distributions of eight morphometric traits and four PC scores from individual larvae reared under four treatment conditions. Boxplots are color coded by treatment condition. The thick horizontal line within each box represents the median value, the box edges represent the 25th and 75th percentiles, vertical lines represent the highest and lowest non-outlying values, and the individual points represent values outside the 95% CI.

and dry mass (Table S2). PC2 scores were significantly higher under high P_{CO_2} conditions (LMM, $P=0.008$; Table S3, Fig. 4). While an interactive effect with temperature was not detected, the effect was more apparent in ambient temperature replicates, where hatchlings exposed to high P_{CO_2} were heavier (+10%) and retained larger yolk sacs (+21%) compared with fish from low P_{CO_2} treatments (Fig. 4). However, when tested individually in a two-way ANOVA, the effect of P_{CO_2} was not significant for either yolk sac area ($P=0.086$) or dry mass ($P=0.297$; Table S3). Thus, PC2 represents the linked variation between yolk sac size and dry mass; that is, hatchlings from high P_{CO_2} were slightly heavier because they hatched with larger yolks compared with their low P_{CO_2} conspecifics.

PC3 accounted for a small amount of total variance (8.9%) that was positively associated with standard length and eye width, but negatively correlated with head width and post-yolk body depth (Table S1). Heatwave conditions significantly reduced PC3 scores (LMM, $P=0.001$; Table S3, Fig. 4) and PC3 was not affected by P_{CO_2} (Table S3, Fig. 4). This indicates that there was a small tendency for heatwave-exposed larvae to develop wider skulls and a deeper body depth while growing to a shorter length with smaller eyes relative to ambient offspring. PC4 account for 6.2% of total variance in morphometric traits and was only associated with variation in eye width (Table S2) and PC4 was unaffected by treatment conditions (Table S2, Fig. 4).

Treatment effects on physiological rates
Under the ambient temperature regime, embryonic RMR increased linearly with developmental day (~20% day^{-1}, ANOVA, $P<0.001$; Table 3, Fig. 5) and exposure to high P_{CO_2} significantly reduced RMR by an average of 6.3% across measurement days (ANOVA, $P=0.006$; Table 3, Fig. 5). For embryos exposed to a progressively warming heatwave environment, RMR increased by 39% from 6 to 7 dpf (11 to 12.2°C) (ANOVA, $P<0.001$; Table 3, Fig. 5). From 7 to

8 dpf (12.2° to 13.2°C), RMR again increased significantly (ANOVA, $P<0.001$; Table 3) but the change (+11%) was relatively small compared with the increase observed from 6 to 7 dpf and the average daily increase under ambient conditions. Overall, there was no effect of P_{CO_2} in embryos exposed to heatwave conditions. When compared on the same day of sampling, heatwave-exposed embryos had significantly higher RMRs on days 6 (+23%, ANOVA: $P<0.001$), 7 (+44%, ANOVA: $P<0.001$) and 8 (+34%, ANOVA: $P<0.001$) post-fertilization (Table 3, Fig. 5). A significant temperature×P_{CO_2} interaction was only detected at 8 dpf (ANOVA, $P=0.014$; Table 3), where high

Table 3. ANOVA results for log-transformed routine metabolic rate (RMR; nmol O$_2$ embryo^{-1} h^{-1} mm^{-2})

Temperature	Factor	d.f.	F	P
Ambient	P_{CO_2}	1	9.658	**0.006**
	Age	2	92.261	**<0.001**
	P_{CO_2}×age	2	1.988	0.166
Heatwave	P_{CO_2}	1	0.044	0.837
	Age	2	107.712	**<0.001**
	P_{CO_2}×age	2	0.251	0.781
Age (dpf)	Factor	d.f.	F	P
6	P_{CO_2}	1	3.126	0.102
	Temperature	1	30.383	**<0.001**
	P_{CO_2}×temperature	1	1.712	0.214
7	P_{CO_2}	1	0.020	0.891
	Temperature	1	208.754	**<0.001**
	P_{CO_2}×temperature	1	0.343	0.569
8	P_{CO_2}	1	1.752	0.210
	Temperature	1	354.712	**<0.001**
	P_{CO_2}×temperature	1	8.230	**0.014**

Results are shown for P_{CO_2}×age effects within temperature regimes and P_{CO_2}×temperature effects by age. Significant treatment effects are denoted in bold.
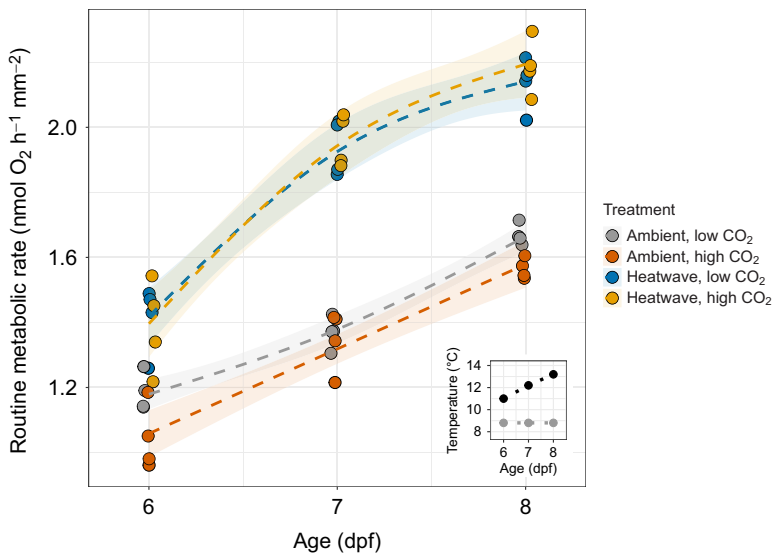
**Fig. 5. Embryonic routine metabolic rate (RMR; nmol O_2 h^{-1} mm^{-2}).** Varying colors denote different treatments. Points represent individual embryo RMR measured from each replicate tank per developmental day. Dotted lines indicate a general additive model fit for each treatment across days and shaded areas denote 1 s.e.m. The inset shows temperature conditions of ambient (gray circles) and heatwave (black circles) treatments for each measurement day.

P_{CO_2} depressed RMR under ambient but not heatwave conditions (Fig. 5).

Q_{10} coefficients calculated for embryos at 60 ddpf showed that a heatwave intensity of +2.3°C induced a relatively modest increase in RMR with a mean Q_{10} value of 1.15, with little variation between P_{CO_2} treatments (Fig. 6). At 70 ddpf, the heatwave intensity increased to +3.5°C above ambient and the mean Q_{10} for RMR increased to 1.72 (Fig. 6). Bootstrapped CIs indicated the Q_{10} values for 70 ddpf embryos were significantly higher in offspring exposed

to high P_{CO_2} (s.e.m.=0.20, Z=2.01, P=0.044). This effect was primarily the result of high P_{CO_2} depressing RMR under ambient temperature conditions while under heatwave conditions P_{CO_2} level had no effect on RMR (Fig. 5).

Developmental rate increased from 6.8±0.2% day^{-1} under ambient temperature conditions to 8.9±0.6% day^{-1} in the heatwave treatments (Fig. 7), which corresponds to an average Q_{10} coefficient of 3.01 (Fig. 6). Exposure to high P_{CO_2} slowed developmental rate by 0.4% day^{-1} under the ambient temperature
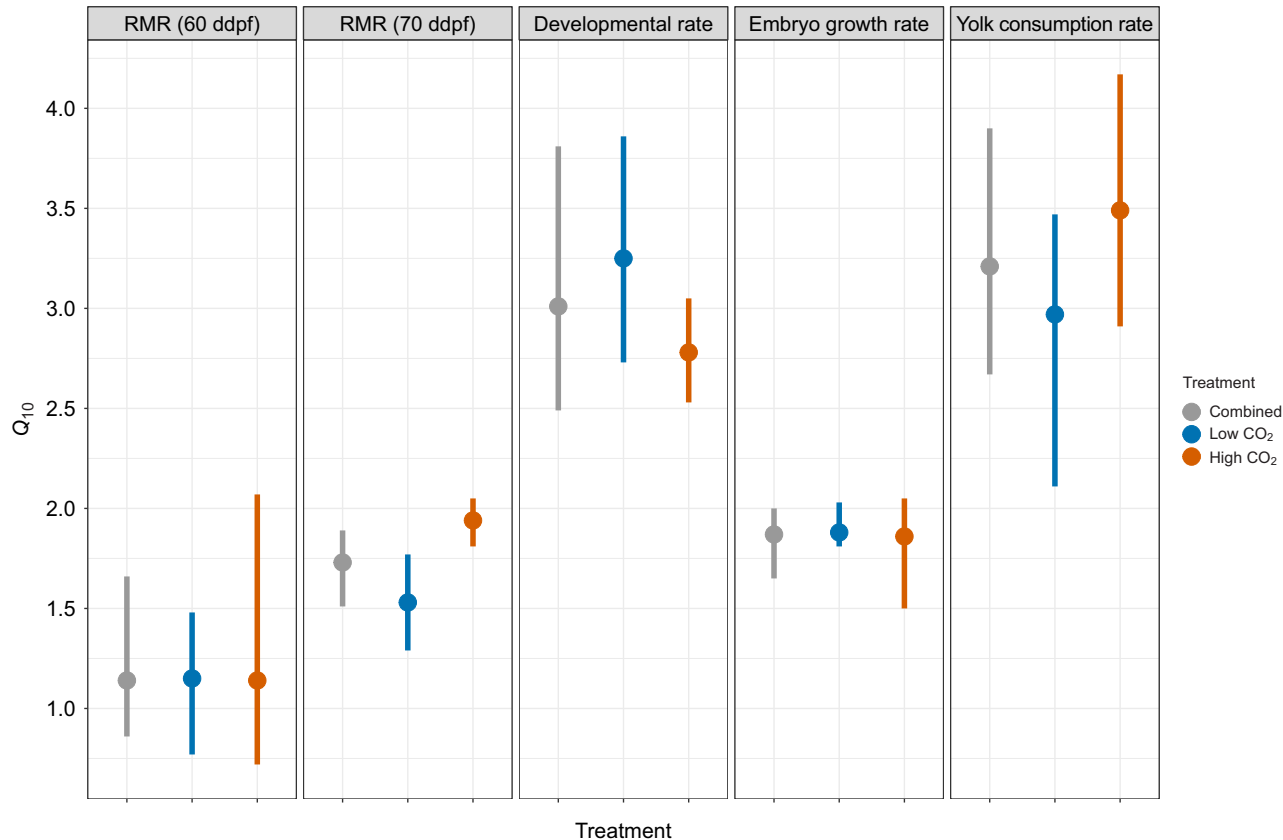
Fig. 6. Summary of Q_{10} coefficients by trait. Mean Q_{10} values (circles) ±95% bootstrapped CIs (vertical lines) for embryo RMR (60 and 70 ddpf, nmol O_2 h^{-1} mm^{-2}), developmental rate (% day^{-1}), embryo growth rate (mm day^{-1}) and yolk consumption rate (% day^{-1}).
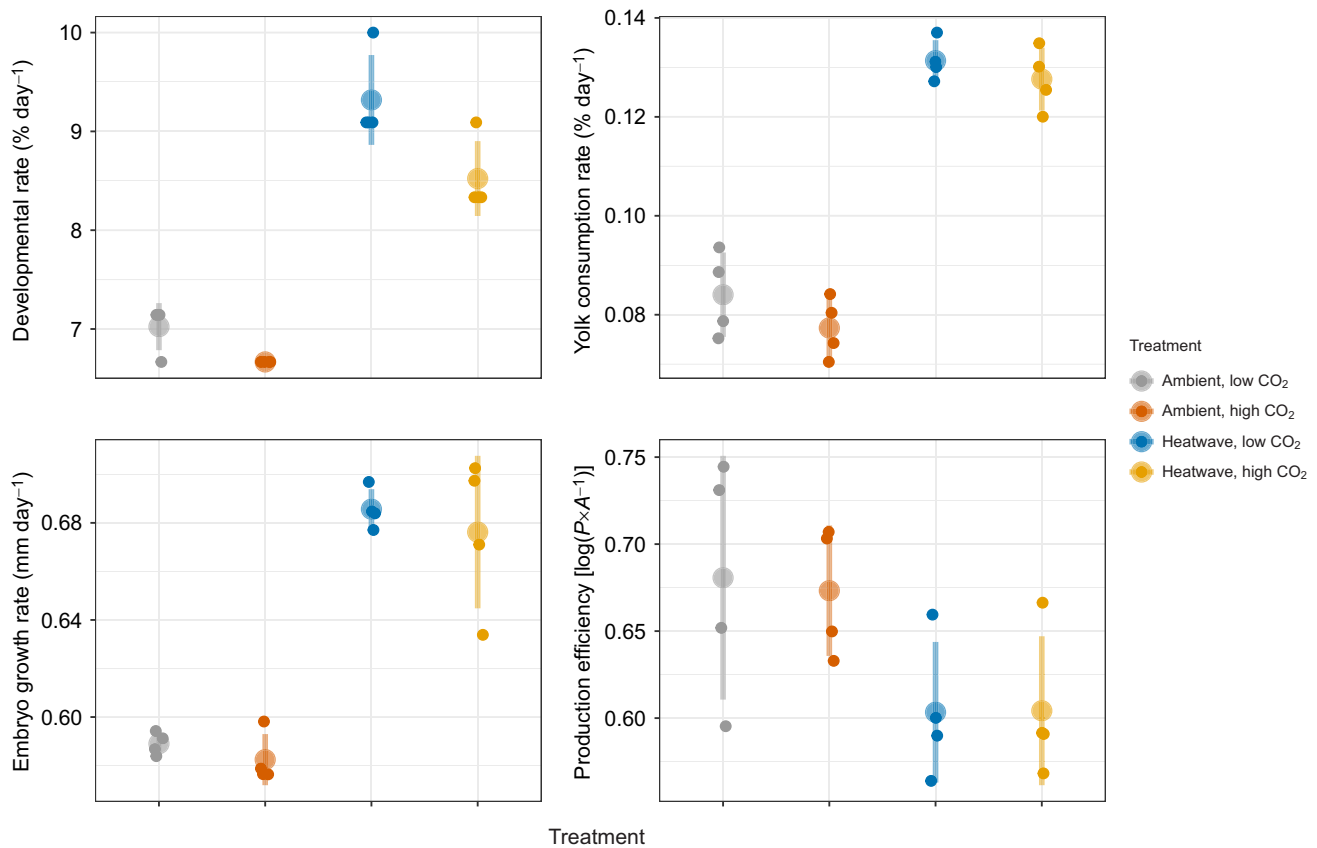
Fig. 7. Developmental rate, yolk consumption rate, embryo growth rate and production efficiency of *C. pallasii* under four treatment conditions. Large colored circles with vertical lines represent treatment means±s.d. Small circles show values for individual replicates.

and by 0.8% d^{-1} in heatwave regime (Fig. 7). This led to a higher average Q_{10} value under low P_{CO_2} conditions, but bootstrapped CIs were not significantly different between P_{CO_2} treatments (s.e.m.=0.26, Z=1.82, P=0.068, Fig. 6). Embryo growth rates were significantly faster under the heatwave (0.68±0.02 mm day^{-1}) versus ambient conditions (0.59±0.01 mm day^{-1}) (ANOVA, P<0.001; Fig. 7, Table S3) which corresponds to a mean Q_{10} of 1.87 (Fig. 6). Growth rate was not statistically affected by P_{CO_2} (Table S3).

Heatwave exposure significantly increased yolk consumption rate to 12.9±0.5% day^{-1} relative to a mean of 8.0±0.8% day^{-1} observed under ambient conditions (ANOVA, P<0.0001; Table S3, Fig. 7) which corresponded to a mean Q_{10} of 3.21 (Fig. 6). This increase in consumption led to a significant reduction (−27%) in the size of remaining yolk reserves at hatch of heatwave offspring compared with ambient conspecifics (LMM, P<0.001; Table S3, Fig. 4). Yolk consumption rates were very similar between P_{CO_2} treatments under the heatwave, but under the ambient temperature, exposure to high P_{CO_2} reduced yolk consumption rate by 9%; however, the effect was not significant (Table S3, Fig. 7). Exposure to the heatwave significantly reduced production efficiency by 10.8%, indicating that heatwave-exposed embryos consumed a greater fraction of yolk reserves to achieve a smaller size at hatch relative to ambient offspring (ANOVA, P=0.012; Table S3, Fig. 7). Production efficiency was not influenced by P_{CO_2} level (Table S3, Fig. 7).

DISCUSSION
Energy metabolism was unaffected by high P_{CO_2}
We hypothesized that (1) exposure to high P_{CO_2} would increase the aerobic respiration of embryos in order to support the increased

biosynthesis of acid–base regulatory factors and (2) this effect would limit the pool of energy available to support higher metabolic rates under heatwave conditions, which would compromise metabolic efficiency and increase mortality. However, after repeatedly measuring $\dot{M}_{O_2}$ during the onset of heatwave conditions, we found no evidence that exposure to 2300 µatm P_{CO_2} increased routine metabolic rates above control P_{CO_2} conditions. This lack of CO_2 effects on metabolism was corroborated by other measured traits: high P_{CO_2} did not increase the rate of yolk consumption or reduce production efficiency and size at hatch in either temperature group. We should not discount the possibility that acclimatization to high P_{CO_2} involved subtle molecular changes, such as preferential expression of more efficient regulatory pathways which could not be detected by the methods employed by this study (Kwan et al., 2021). However, regardless of the mechanism, it appears that Pacific herring offspring have a high intrinsic capacity for acid–base regulation that does not require a large energetic investment. Furthermore, this capacity means that high P_{CO_2} did not increase embryo mortality by limiting the amount of energy available for thermal acclimation. This finding contrasts with a recent study of Pacific herring in which exposure to ~1200 µatm P_{CO_2} significantly elevated the rate of embryonic heartbeats by ~10% at 16°C but not at 10°C (Villalobos et al., 2020). Notably, embryo survival was quite low at 16°C (~25%), so synergistic effects on metabolic rate in this species might only occur when temperatures approach or exceed upper critical limits, which were not tested in this study (Dahlke et al., 2017).

Significant effects of high P_{CO_2} were limited; exposure to 2300 µatm increased time to hatch by ~1 day in both temperature

groups and reduced routine metabolic rate by 6.3% under the ambient temperature regime only. These effects were accompanied by small and non-significant effects of high CO_2, such as slower growth and yolk consumption, including a 9% reduction in the rate of yolk consumption under the ambient temperature. The mechanism underlying this slight metabolic depression is unclear, as the level of P_{CO_2} required to induce an anesthetic response is thought to be orders of magnitude higher than what was applied here (Lefevre, 2019). High P_{CO_2} also increased time to hatch in embryos of the northern sand lance, *Ammodytes dubius*, where the delay was thought to be caused by low pH interfering with the hatching process directly (Murray et al., 2019). Regardless of the mechanism, a longer time to hatch is unlikely to be adaptive because it would exacerbate the very high rates of predation inflicted upon Pacific herring eggs (Keeling et al., 2017). However, these small effects should not be overstated and our findings join the bulk of experimental evidence showing that high P_{CO_2} conditions consistent with near-future ocean conditions have limited effects (<±10%) on the physiological rates of most marine fish embryos (Flynn et al., 2015; Lefevre, 2019; Leo et al., 2018; Schwemmer et al., 2020).

The effect of high P_{CO_2} on embryo mortality was more complex. Hatching success was very similar between P_{CO_2} treatments under the ambient regime (75–76%) but in heatwave-exposed replicates it was 11% higher under low (86%) compared with high P_{CO_2} (75%). Although the interactive effect was marginally insignificant, the measured difference in survival under the heatwave regime was triggered by a higher total hatch and a lower rate of developmental anomalies under low P_{CO_2}. Teratogenic effects under high P_{CO_2} have been observed in other clupeid early life stages. Exposure to ~1100 μatm P_{CO_2} more than doubled the incidence of malformations in Atlantic herring embryos, with up to 17% of hatchlings showing anomalies when tested across a range of temperatures (Leo et al., 2018). High rates of organ damage were also observed in 3-week-old Atlantic herring larvae reared continuously under ~2000 μatm P_{CO_2} (Frommel et al., 2014). Furthermore, exposure to ~1200 μatm P_{CO_2} increased the rate of mortality by 10% in Pacific herring embryos when simultaneously exposed to 16°C, but anomaly rates were not quantified in that study (Villalobos et al., 2020). Thus, there is accumulating evidence that high P_{CO_2} may increase teratogenic effects in clupeid species by impairing normal developmental trajectories. The precise mechanisms involved warrant further examination.

Heatwave impacts: survival was robust but metabolic efficiency declined

Our analysis of the long-term NERRS data from Padilla Bay, WA, found that nearshore heatwaves can occur during all months of the year and therefore have the potential to impact herring spawning events throughout the reproductive season. Although most years of the time series exhibited just one or two events, the period covering the 2014–2016 North Pacific Heatwave Event showed a spike in activity with 26 nearshore events occurring over just 3 years (see Supplementary Materials and Methods). Seven of top 10 most extreme heatwaves were detected during this period. We modeled the simulated heatwave of the experiment after these extreme events with the expectation that embryo survival would decline as temperatures reached maximum intensity, based on an established thermal reaction norm derived from static-temperature experiments on Salish Sea herring (Alderdice and Velsen, 1971). Contrary to our expectation, heatwave exposure actually increased total hatch counts, but the simultaneous increase to the rate of developmental anomalies acted to reduce overall hatching

success to a rate similar to that observed in the ambient temperature regime.

The observed higher-than-expected survival was likely due to the specific timing of the thermal challenge: the heatwave was initiated after embryos had developed under ambient conditions for ~3.5 dpf and maximum intensity was reached when embryos had attained 75% of full development. This suggests the Pacific herring, like other temperate and cold-water fish, are most stenothermal during the earliest phases of embryogenesis (i.e. during gastrulation) and limits of thermal tolerance expand throughout organogenesis (Dahlke et al., 2020a; Flynn and Todgham, 2018; Mueller et al., 2015). As such, Pacific herring embryos were able to outgrow the lethal effects of our simulated heatwave despite being sourced from a population that reproduces in February and early March, when daily mean temperatures are relatively cold and diel variability is low (8.1±1.2°C) (Sandell et al., 2019). These results suggest that winter-spawning Salish Sea herring retain sufficient thermal plasticity to survive a relatively extreme heatwave event, but whether earlier embryonic stages are more sensitive to the thermal stress of a developing heatwave requires further examination.

The heatwave affected most measured physiological rates, but to varying degrees. For example, rate of development to hatch (Q_{10}=3.01) was not matched by a proportional increase in embryonic growth rate (Q_{10}=1.87). This means that despite a faster growth rate, larvae from the heatwave regime were ~10% smaller at hatch than their conspecifics reared at ambient temperatures. This is consistent with previous findings from Pacific herring (Alderdice and Velsen, 1971; Dinnel et al., 2010; Villalobos et al., 2020) and fits within the broader pattern exhibited by temperate fish of an inverse relationship between hatch size and temperature (Rombough, 1997). It is also assumed that temperature has proportionally equal effect on the rates of growth and yolk consumption, such that production efficiency (i.e. the ratio of tissue produced to yolk assimilated) tends to be insensitive to temperature change within a species' thermal envelope (Houde, 1989; Rombough, 2011). This is a key metabolic relationship, as it enables embryos to achieve exceptionally high specific growth rates via the efficient conversion of maternally derived yolk reserves into new embryonic tissue (Kamler, 2008; Rombough, 2006).

However, we found that heatwave-exposed embryos exhibited a 10.8% reduction in production efficiency as the Q_{10} coefficient for yolk consumption (Q_{10}=3.21) and was substantially greater than the estimate for growth rate. In effect, this meant that heatwave-exposed embryos consumed a larger fraction of their yolk supply to achieve a smaller body size at hatch. This finding is somewhat contradictory with the modest Q_{10} coefficients we estimated for RMR during the onset of the heatwave (Q_{10}=1.17 at +2.3°C and Q_{10}=1.70 at +3.5°C). We would have expected a greater effect on RMR to induce a loss of production efficiency, particularly given that fish embryos typically exhibit Q_{10} coefficients close to 3.0 (Rombough, 2011). However, we could not assess the Q_{10} for RMR at maximum heatwave intensity (+4.4°C) as the handling required to make the measurements induced hatching in late-stage embryos, but it is probable that it continued to increase as Q_{10} values for oxygen demand tend to closely align with yolk utilization rates (Houde, 1989; Rombough, 2011). This is consistent with findings from the lake whitefish (*Coregonus clupeaformis*), where cost of development (which encompasses all energetic processes) showed the largest increase with temperature during the ladder stages of embryogenesis (Mueller et al., 2015).

The higher incidence of developmental anomalies under the heatwave conditions suggests that some embryos were suffering

cellular damage related to thermal stress (Basu et al., 2002). Thus, the observed production inefficiencies may be related to the energetically intensive processes related to countering heat stress. As standard metabolic rates increase with warming, additional energetic costs accumulate with the increased biosynthesis of heat shock proteins (Alfonso et al., 2021; Takle et al., 2005). A metabolic trade-off to preserve cellular integrity at the expense of growth could negatively influence recruitment dynamics because higher rates of predation and starvation are inversely correlated with larval size (Hendry et al., 2001; Miller et al., 1988, but see Pepin, 1991). Furthermore, lingering growth deficiencies induced during embryogenesis could be exacerbated during larval and juvenile growth owing to large-scale ecosystem disruption and changes in predator and prey dynamics that accompany prolonged heatwave events (von Biela et al., 2019). Particularly at risk is the Cherry Point herring population, which spawns later than all other herring stocks in the Salish Sea, reaching peak activity in mid-May (Sandell et al., 2019), when nearshore temperatures are warmer and more variable (13.5±2.6°C) compared with conditions for winter spawners and the risk for high intensity heatwaves appears to be greatest in late spring. Despite this late spawning phenology, a recent study on the genetic diversity of Salish Sea herring found no evidence for thermal adaptation in the Cherry Point stock (Petrou et al., 2021), suggesting that embryos are already developing near their maximal thermal limits. The Cherry Point stock was once the largest in the region but has suffered severe declines in recent years (Sandell et al., 2019). Rising ocean temperatures and the emergence of intense regional heatwaves may now be constraining the reproductive viability of this unique population.

Conclusions and future directions

We found that Pacific herring embryos could successfully acclimate to the stimulated heatwave without a reduction in survival, even when simultaneously exposed to high P_{CO_2} conditions. The effects of high P_{CO_2} were minimal and we found no evidence that acidification increased aerobic respiration or increased energy expenditure towards acid–base regulation. However, the heatwave did elicit measurable metabolic trade-offs, including a significant reduction in the production efficiency of developing embryos, resulting in a smaller size at hatch with smaller yolk reserves. Quantifying how these effects will impact the fitness of wild offspring will require long-term studies that can properly assess carryover effects to later life stages. Furthermore, these experimental data need to be synthesized with field observations of community-level heatwave responses to understand the dynamic effects on the predators and prey of herring larvae.

There is a growing understanding that fluctuating environments elicit different physiological responses compared with static environments with the same average values (Cross et al., 2019; Schunter et al., 2021; Tomasetti et al., 2021), necessitating that environmental variability be incorporated into experimental designs (Kroeker et al., 2020; Morash et al., 2018). Although the present study provides critical data on the influence of a developing heatwave, our experimental treatments did not simulate the full complexity of nearshore habitats. For example, high-frequency variations of temperature and P_{CO_2} that fluctuate over diel and tidal cycles are ubiquitous in shallow coastal marine systems (Baumann and Smith, 2017; Pacella et al., 2018). Extreme heatwaves that increase daily mean temperatures will also increase the amplitude of these fluctuations and extend the duration of extreme conditions (Schlegel et al., 2017; Wetz and Yoskowitz, 2013; Zhang et al., 2013). Biological proofs of Jensen's inequality tell us that

organismal performance under variable environments is lower than under static conditions of the same mean, and that performance continues to decline as variability increases (Denny, 2017; Morash et al., 2018). Therefore, it is possible that the outcomes of this study could be different if high-frequency fluctuations of temperature and P_{CO_2} were superimposed on top of the daily heatwave progression. This could be addressed by future investigations specifically designed to assess the phenotypic effects of high-frequency exposures to extreme conditions.

References

Alderdice, D. F. and Hourston, A. S. (1985). Factors influencing development and survival of pacific herring (*Clupea harengus pallasi*) eggs and larvae to beginning of exogenous feeding. *Can. J. Fish. Aquat. Sci.* **42**, s56-s68. doi:10.1139/f85-262

Alderdice, D. F. and Velsen, F. P. J. (1971). Some effects of salinity and temperautre on early development of pacific herring (*Clupea pallasi*). *J. Fish. Res. Board Can.* **28**, 1545-1562. doi:10.1139/f71-234

Alfonso, S., Gesto, M. and Sadoul, B. (2021). Temperature increase and its effects on fish stress physiology in the context of global warming. *J. Fish Biol.* **98**, 1496-1508. doi:10.1111/jfb.14599

Altman, D. G. and Bland, J. M. (2011). How to obtain the P value from a confidence interval. *BMJ* **343**, d2304. doi:10.1136/bmj.d2304

Basu, N., Todgham, A. E., Ackerman, P. A., Bibeau, M. R., Nakano, K., Schulte, P. M. and Iwama, G. K. (2002). Heat shock protein genes and their functional significance in fish. *Gene* **295**, 173-183. doi:10.1016/S0378-1119(02)00687-X

Bates, D., Mächler, M., Bolker, B. and Walker, S. (2015). Fitting linear mixed-effects models using lme4. *J. Stat. Soft.* **67**, 1-48.

Baumann, H. (2019). Experimental assessments of marine species sensitivities to ocean acidification and co-stressors: how far have we come? *Can. J. Zool.* **97**, 399-408. doi:10.1139/cjz-2018-0198

Baumann, H. and Smith, E. M. (2017). Quantifying metabolically driven pH and oxygen fluctuations in US nearshore habitats at diel to interannual time scales. *Estuaries Coasts* **41**, 1102-1117. doi:10.1007/s12237-017-0321-3

Bond, N. A., Cronin, M. F., Freeland, H. and Mantua, N. (2015). Causes and impacts of the 2014 warm anomaly in the NE Pacific. *Geophys. Res. Lett.* **42**, 3414-3420. doi:10.1002/2015GL063306

Brauner, C. J., Shartau, R. B., Damsgaard, C., Esbaugh, A. J., Wilson, R. W. and Grosell, M. (2019). Acid-base physiology and CO_2 homeostasis: regulation and compensation in response to elevated environmental CO_2. In *Fish Physiology*, Vol. 37 (ed. M. Grosell, P. L. Munday, A. P. Farrell and C. J. Brauner), pp. 69-132. Academic Press.

Bulthuis, D. A. (2013). *The Ecology of Padilla Bay, Washington: An Estuarine Profile of a National Estuarine Research Reserve*. Mount Vernon, WA: Washington State Department of Ecology.

Burggren, W. (2018). Developmental phenotypic plasticity helps bridge stochastic weather events associated with climate change. *J. Exp. Biol.* **221**, jeb161984. doi:10.1242/jeb.161984

Cattano, C., Giomi, F. and Milazzo, M. (2016). Effects of ocean acidification on embryonic respiration and development of a temperate wrasse living along a natural CO_2 gradient. *Conserv. Physiol.* **4**, cov073. doi:10.1093/conphys/cov073

Cross, E. L., Murray, C. S. and Baumann, H. (2019). Diel and tidal $pCO_2 \times O_2$ fluctuations provide physiological refuge to early life stages of a coastal forage fish. *Sci. Rep.* **9**, 18146. doi:10.1038/s41598-019-53930-8

Dahlke, F. T., Leo, E., Mark, F. C., Pörtner, H. O., Bickmeyer, U., Frickenhaus, S. and Storch, D. (2017). Effects of ocean acidification increase embryonic sensitivity to thermal extremes in Atlantic cod, *Gadus morhua*. *Glob. Change Biol.* **23**, 1499-1510. doi:10.1111/gcb.13527

Dahlke, F. T., Butzin, M., Nahrgang, J., Puvanendran, V., Mortensen, A., Pörtner, H.-O. and Storch, D. (2018). Northern cod species face spawning habitat losses if global warming exceeds 1.5°C. *Sci. Adv.* **4**, eaas8821. doi:10.1126/sciadv.aas8821

Dahlke, F., Lucassen, M., Bickmeyer, U., Wohlrab, S., Puvanendran, V., Mortensen, A., Chierici, M., Pörtner, H.-O. and Storch, D. (2020a). Fish embryo vulnerability to combined acidification and warming coincides with low capacity for homeostatic regulation. *J. Exp. Biol.* **223**, jeb212589. doi:10.1242/jeb.212589

Dahlke, F. T., Wohlrab, S., Butzin, M. and Pörtner, H.-O. (2020b). Thermal bottlenecks in the life cycle define climate vulnerability of fish. *Science* **369**, 65-70. doi:10.1126/science.aaz3658

Denny, M. (2017). The fallacy of the average: on the ubiquity, utility and continuing novelty of Jensen's inequality. *J. Exp. Biol.* **220**, 139-146. doi:10.1242/jeb.140368

Di Lorenzo, E. and Mantua, N. (2016). Multi-year persistence of the 2014/15 North Pacific marine heatwave. *Nature Climate Change* **6**, 1042-1047. doi:10.1038/nclimate3082

Dickson, A. G. (1990). Standard potential of the reaction: $AgCl(s)+12H_2(g)=Ag(s)+HCl(aq)$, and the standard acidity constant of the ion HSO_4- in synthetic sea water from 273.15 to 318.15 K. *J. Chem. Thermodynamics* **22**, 113-127. doi:10.1016/0021-9614(90)90074-Z

Dickson, A. G. and Millero, F. J. (1987). A comparison of the equilibrium constants for the dissociation of carbonic acid in seawater media. *Deep Sea Res. A Oceanogr. Res Pap.* **34**, 1733-1743. doi:10.1016/0198-0149(87)90021-5

Dickson, A. G., Sabine, C. L. and Christian, J. R. (2007). Guide to best practices for ocean CO_2 measurements. PICES Special Publication 3. IOCCP Report 8.

Dickson, A. G., Camões, M. F., Spitzer, P., Fisicaro, P., Stoica, D., Pawlowicz, R. and Feistel, R. (2015). Metrological challenges for measurements of key climatological observables. Part 3: seawater pH. *Metrologia* **53**, R26-R39. doi:10.1088/0026-1394/53/1/R26

Dinnel, P. A., Middaugh, D. P., Schwarck, N. T., Farren, H. M., Haley, R. K., Hoover, R. A., Elphick, J., Tobiason, K. and Marshall, R. R. (2010). Methods for conducting bioassays using embryos and larvae of Pacific herring, *Clupea pallasi*. *Arch. Environ. Contam. Toxicol.* **60**, 290-308. doi:10.1007/s00244-010-9600-8

Esbaugh, A. J. (2018). Physiological implications of ocean acidification for marine fish: emerging patterns and new insights. *J. Comp. Physiol. B* **188**, 1-13. doi:10.1007/s00360-017-1105-6

Evans, W., Pocock, K., Hare, A., Weekes, C., Hales, B., Jackson, J., Gurney-Smith, H., Mathis, J. T., Alin, S. R. and Feely, R. A. (2019). Marine CO_2 patterns in the Northern Salish Sea. *Front. Mar. Sci.* **5**, 00536. doi:10.3389/fmars.2018.00536

Fassbender, A. J., Alin, S. R., Feely, R. A., Sutton, A. J., Newton, J. A. and Byrne, R. H. (2016). Estimating total alkalinity in the Washington state coastal zone: complexities and surprising utility for ocean acidification research. *Estuaries Coasts* **40**, 404-418. doi:10.1007/s12237-016-0168-z

Fassbender, A. J., Alin, S. R., Feely, R. A., Sutton, A. J., Newton, J. A., Krembs, C., Bos, J., Keyzers, M., Devol, A., Ruef, W. et al. (2018). Seasonal carbonate chemistry variability in marine surface waters of the US Pacific Northwest. *Earth System Sci. Data* **10**, 1367-1401. doi:10.5194/essd-10-1367-2018

Feely, R. A., Alin, S. R., Newton, J., Sabine, C. L., Warner, M., Devol, A., Krembs, C., Maloy, C. (2010). The combined effects of ocean acidification, mixing, and respiration on pH and carbonate saturation in an urbanized estuary. *Estuar. Coast. Shelf Sci.* **88**, 442-449. doi:10.1016/j.ecss.2010.05.004

Fisher, J., Kimmel, D., Ross, T., Batten, S., Bjorkstedt, E., Galbraith, M., Jacobson, K., Keister, J., Sastri, A. and Suchy, K. (2020). Copepod responses to, and recovery from, the recent marine heatwave in the Northeast Pacific. *PICES Science in 2019: Notes from the Science Board Chair* **28**, 65.

Flynn, E. E. and Todgham, A. E. (2018). Thermal windows and metabolic performance curves in a developing Antarctic fish. *J. Comp. Physiol. B* **188**, 271-282. doi:10.1007/s00360-017-1124-3

Flynn, E. E., Bjelde, B. E., Miller, N. A. and Todgham, A. E. (2015). Ocean acidification exerts negative effects during warming conditions in a developing Antarctic fish. *Conserv. Physiol.* **3**, cov033. doi:10.1093/conphys/cov033

Fox, R. J., Donelson, J. M., Schunter, C., Ravasi, T. and Gaitán-Espitia, J. D. (2019). Beyond buying time: the role of plasticity in phenotypic adaptation to rapid environmental change. *Philos. Trans. R. Soc. B Biol. Sci.* **374**, 20180174. doi:10.1098/rstb.2018.0174

Franke, A. and Clemmesen, C. (2011). Effect of ocean acidification on early life stages of Atlantic herring (*Clupea harengus* L.). *Biogeosciences* **8**, 3697-3707. doi:10.5194/bg-8-3697-2011

Frölicher, T. L., Fischer, E. M. and Gruber, N. (2018). Marine heatwaves under global warming. *Nature* **560**, 360-364. doi:10.1038/s41586-018-0383-9

Frommel, A. Y., Maneja, R., Lowe, D., Pascoe, C. K., Geffen, A. J., Folkvord, A., Piatkowski, U. and Clemmesen, C. (2014). Organ damage in Atlantic herring larvae as a result of ocean acidification. *Ecol. Appl.* **24**, 1131-1143. doi:10.1890/13-0297.1

Gentemann, C. L., Fewings, M. R. and García-Reyes, M. (2017). Satellite sea surface temperatures along the West Coast of the United States during the 2014–2016 northeast Pacific marine heat wave. *Geophys. Res. Lett.* **44**, 312-319. doi:10.1002/2016GL071039

Hay, D. E. (1985). Reproductive biology of Pacific herring (*Clupea harengus pallasi*). *Can. J. Fish. Aquat. Sci.* **42**, s111-s126. doi:10.1139/f85-267

Hendry, A. P., Day, T. and Cooper, A. B. (2001). Optimal size and number of propagules: allowance for discrete stages and effects of maternal size on reproductive output and offspring fitness. *Am. Nat.* **157**, 387-407. doi:10.1086/319316

Hershberger, P. K., Elder, N. E., Wittouck, J., Stick, K. and Kocan, R. M. (2005). Abnormalities in larvae from the once-largest pacific herring population in Washington state result primarily from factors independent of spawning location. *Trans. Am. Fish. Soc.* **134**, 326-337. doi:10.1577/T03-227.1

Heuer, R. M. and Grosell, M. (2016). Elevated CO_2 increases energetic cost and ion movement in the marine fish intestine. *Sci. Rep.* **6**, 34480. doi:10.1038/srep34480

Hobday, A. J., Alexander, L. V., Perkins, S. E., Smale, D. A., Straub, S. C., Oliver, E. C. J., Benthuysen, J. A., Burrows, M. T., Donat, M. G., Feng, M. et al. (2016). A hierarchical approach to defining marine heatwaves. *Prog. Oceanogr.* **141**, 227-238. doi:10.1016/j.pocean.2015.12.014

Hobday, A. J., Oliver, E. C., Gupta, A. S., Benthuysen, J. A., Burrows, M. T., Donat, M. G., Holbrook, N. J., Moore, P. J., Thomsen, M. S. and Wernberg, T. (2018). Categorizing and naming marine heatwaves. *Oceanography* **31**, 162-173. doi:10.5670/oceanog.2018.205

Houde, E. D. (1989). Comparative growth, mortality, and energetics of marine fish larvae: temperature and implied latitudinal effects. *Fish. Bull.* **87**, 471-495.

Jonsson, B. and Jonsson, N. (2019). Phenotypic plasticity and epigenetics of fish: embryo temperature affects later-developing lift-history traits. *Aquat. Biol.* **28**, 21-32. doi:10.3354/ab00707

Kamler, E. (2008). Resource allocation in yolk-feeding fish. *Rev. Fish Biol. Fish.* **18**, 143. doi:10.1007/s11160-007-9070-x

Kawakami, T., Okouchi, H., Aritaki, M., Aoyama, J. and Tsukamoto, K. (2011). Embryonic development and morphology of eggs and newly hatched larvae of Pacific herring *Clupea pallasii*. *Fish. Sci.* **77**, 183-190. doi:10.1007/s12562-010-0317-4

Keeling, B., Hessing-Lewis, M., Housty, C., Okamoto, D. K., Gregr, E. J. and Salomon, A. K. (2017). Factors driving spatial variation in egg survival of an ecologically and culturally important forage fish. *Aquat. Conserv. Mar. Freshw. Ecosyst.* **27**, 814-827. doi:10.1002/aqc.2757

Kreiss, C. M., Michael, K., Bock, C., Lucassen, M. and Pörtner, H.-O. (2015). Impact of long-term moderate hypercapnia and elevated temperature on the energy budget of isolated gills of Atlantic cod (*Gadus morhua*). *Comp. Biochem. Physiol. A Mol. Integr. Physiol.* **182**, 102-112. doi:10.1016/j.cbpa.2014.12.019

Kroeker, K. J., Bell, L. E., Donham, E. M., Hoshijima, U., Lummis, S., Toy, J. A. and Willis-Norton, E. (2020). Ecological change in dynamic environments: accounting for temporal environmental variability in studies of ocean change biology. *Glob. Change Biol.* **26**, 54-67. doi:10.1111/gcb.14868

Kuznetsova, A., Brockhoff, P. B. and Christensen, R. H. B. (2017). lmerTest package: tests in linear mixed effects models. *J. Stat. Softw.* **82**, 1-26. doi:10.18637/jss.v082.i13

Kwan, G. T., Shen, S. G., Drawbridge, M., Checkley, D. M. and Tresguerres, M. (2021). Ion-transporting capacity and aerobic respiration of larval white seabass (*Atractoscion nobilis*) may be resilient to ocean acidification conditions. *Sci. Total Environ.* **791**, 148285. doi:10.1016/j.scitotenv.2021.148285

Lefevre, S. (2016). Are global warming and ocean acidification conspiring against marine ectotherms? A meta-analysis of the respiratory effects of elevated temperature, high CO_2 and their interaction. *Conserv. Physiol.* **4**, cow009. doi:10.1093/conphys/cow009

Lefevre, S. (2019). Effects of high CO_2 on oxygen consumption rates, aerobic scope and swimming performance. In *Fish Physiology*, Vol. 37 (ed. M. Grosell, P. L. Munday, A. P. Farrell and C. J. Brauner), pp. 195-244. Academic Press.

Leo, E., Dahlke, F. T., Storch, D., Pörtner, H.-O. and Mark, F. C. (2018). Impact of ocean acidification and warming on the bioenergetics of developing eggs of Atlantic herring *Clupea harengus*. *Conserv. Physiol.* **6**, coy050. doi:10.1093/conphys/coy050

Love, B. A., Olson, M. B. and Wuori, T. (2017). Technical Note: A minimally invasive experimental system for pCO_2 manipulation in plankton cultures using passive gas exchange (atmospheric carbon control simulator). *Biogeosciences* **14**, 2675-2684. doi:10.5194/bg-14-2675-2017

Mauger, G., Casola, J., Morgan, H., Strauch, R., Jones, B., Curry, B., Busch Isaksen, T., Whitely Binder, L., Krosby, M. and Snover, A. (2015). State of knowledge: Climate change in Puget Sound. In *Report prepared for the Puget Sound Partnership and the National Oceanic and Atmospheric Administration*. Seattle: Climate Impacts Group, University of Washington. doi:10.7915/CIG93777D

Mehrbach, C., Culberson, C. H., Hawley, J. E. and Pytkowicx, R. M. (1973). Measurement of the apparent dissociation constants of carbonic acid in seawater at atmospheric pressure. *Limnol. Oceanogr.* **18**, 897-907. doi:10.4319/lo.1973. 18.6.0897

Melzner, F., Gutowska, M. A., Langenbuch, M., Dupont, S., Lucassen, M., Thorndyke, M. C., Bleich, M. and Pörtner, H.-O. (2009). Physiological basis for high CO_2 tolerance in marine ectothermic animals: pre-adaptation through lifestyle and ontogeny? *Biogeosciences* **6**, 2313-2331. doi:10.5194/bg-6-2313-2009

Merino, G., Barange, M. and Mullon, C. (2010). Climate variability and change scenarios for a marine commodity: modelling small pelagic fish, fisheries and fishmeal in a globalized market. *J. Mar. Syst.* **81**, 196-205. doi:10.1016/j.jmarsys. 2009.12.010

Miller, T. J., Crowder, L. B., Rice, J. A. and Marschall, E. A. (1988). Larval size and recruitment mechanisms in fishes: toward a conceptual framework. *Can. J. Fish. Aquat. Sci.* **45**, 1657-1670. doi:10.1139/f88-197

Mölich, A. and Heisler, N. (2005). Determination of pH by microfluorometry: intracellular and interstitial pH regulation in developing early-stage fish embryos (*Danio rerio*). *J. Exp. Biol.* **208**, 4137-4149. doi:10.1242/jeb.01878

Morash, A. J., Neufeld, C., MacCormack, T. J. and Currie, S. (2018). The importance of incorporating natural thermal variation when evaluating physiological performance in wild species. *J. Exp. Biol.* **221**, jeb164673. doi:10.1242/jeb.164673

Mueller, C. A., Eme, J., Manzon, R. G., Somers, C. M., Boreham, D. R. and Wilson, J. Y. (2015). Embryonic critical windows: changes in incubation temperature alter survival, hatchling phenotype, and cost of development in lake whitefish (*Coregonus clupeaformis*). *J. Comp. Physiol. B* **185**, 315-331. doi:10.1007/s00360-015-0886-8

Murray, C. S. (2022). Experimental data testing CO2 × heatwave effects in Pacific herring offspring including data on vital rates and experimental conditions. *Dryad Dataset.* doi:10.10.5061/dryad.q573n5tkw

Murray, C. S. and Baumann, H. (2018). You better repeat it: complex CO_2×temperature effects in Atlantic silverside offspring revealed by serial experimentation. *Diversity* **10**, 69. doi:10.3390/d10030069

Murray, C. S., Malvezzi, A., Gobler, C. J. and Baumann, H. (2014). Offspring sensitivity to ocean acidification changes seasonally in a coastal marine fish. *Mar. Ecol. Prog. Ser.* **504**, 1-11. doi:10.3354/meps10791

Murray, C. S., Wiley, D. and Baumann, H. (2019). High sensitivity of a keystone forage fish to elevated CO_2 and temperature. *Conser. Physiol.* **7**, coz084. doi:10.1093/conphys/coz084

Pacella, S. R., Brown, C. A., Waldbusser, G. G., Labiosa, R. G. and Hales, B. (2018). Seagrass habitat metabolism increases short-term extremes and long-term offset of CO_2 under future ocean acidification. *Proc. Natl Acad. Sci. USA* **115**, 3870-3875. doi:10.1073/pnas.1703445115

Peck, M. A. and Moyano, M. (2016). Measuring respiration rates in marine fish larvae: challenges and advances. *J. Fish Biol.* **88**, 173-205. doi:10.1111/jfb.12810

Penttila, D. (2007). *Marine Forage Fishes in Puget Sound*. Olympia, WA: Washington Department of Fish and Wildlife.

Pepin, P. (1991). Effect of temperature and size on development, mortality, and survival rates of the pelagic early life history stages of marine fish. *Can. J. Fish. Aquat. Sci.* **48**, 503-518.

Petrou, E. L., Fuentes-Pardo, A. P., Rogers, L. A., Orobko, M., Tarpey, C., Jiménez-Hidalgo, I., Moss, M. L., Yang, D., Pitcher, T. J., Sandell, T. et al. (2021). Functional genetic diversity in an exploited marine species and its relevance to fisheries management. *Proc. R. Soc. B* **288**, 20202398. doi:10.1098/rspb.2020.2398

Piatt, J. F., Parrish, J. K., Renner, H. M., Schoen, S. K., Jones, T. T., Arimitsu, M. L., Kuletz, K. J., Bodenstein, B., García-Reyes, M., Duerr, R. S. et al. (2020). Extreme mortality and reproductive failure of common murres resulting from the northeast Pacific marine heatwave of 2014-2016. *PLoS ONE* **15**, e0226087. doi:10.1371/journal.pone.0226087

Pikitch, E., Boersma, P. D., Boyd, I., Conover, D., Cury, P., Essington, T., Heppell, S., Houde, E., Mangel, M. and Pauly, D. (2012). *Little Fish, Big Impact: Managing a Crucial Link in Ocean Food Webs*. Washington, DC: Lenfest Ocean Program.

Pörtner, H. O. (2008). Ecosystem effects of ocean acidification in times of ocean warming: a physiologist's view. *Mar. Ecol. Prog. Ser.* **373**, 203-217. doi:10.3354/meps07768

Pörtner, H.-O. (2010). Oxygen- and capacity-limitation of thermal tolerance: a matrix for integrating climate-related stressor effects in marine ecosystems. *J. Exp. Biol.* **213**, 881-893. doi:10.1242/jeb.037523

Pörtner, H.-O. and Peck, M. A. (2010). Climate change effects on fishes and fisheries: towards a cause and effect understanding. *J. Fish Biol.* **77**, 1745-1779. doi:10.1111/j.1095-8649.2010.02783.x

Purcell, J., Grosse, D. and Grover, J. (1990). Mass abundances of abnormal pacific herring larvae at a spawning ground in British Columbia. *Trans. Am. Fish. Soc.* **119**, 463-469. doi:10.1577/1548-8659(1990)119<0463:MAOAPH>2.3.CO;2

Rombough, P. J. (1994). Energy partitioning during fish development: additive or compensatory allocation of energy to support growth? *Funct. Ecol.* **8**, 178-186. doi:10.2307/2389901

Rombough, P. J. (1997). The effects of temperature on embryonic and larval development. In *Global Warming: Implications for Freshwater and Marine Fish* (eds. C. M. Wood and D. G. McDonald), pp. 177-224. Cambridge: Cambridge University Press.

Rombough, P. J. (2006). Developmental costs and the partitioning of metabolic energy. In *Comparative Developmental Physiology: Contributions, Tools and Trends* (ed. T. J. Warburton, W. W. Burggren, B. Pelster, C. L. Reiber and J. Spicer), p. 216: Oxford University Press USA - OSO.

Rombough, P. (2011). The energetics of embryonic growth. *Respir. Physiol. Neurobiol.* **178**, 22-29. doi:10.1016/j.resp.2011.04.026

Sandell, T., Lindquist, A., Dionne, P. and Lowry, D. (2019). *2016 Washington State Herring Stock Status Report. Species Status Reports. Fish Program Technical Report No. FPT 19-07*. Olympia, WA: Washington Department of Fish and Wildlife.

Schlegel, R. W. and Smit, A. J. (2018). heatwaveR: A central algorithm for the detection of heatwaves and cold-spells. *J. Open Source Softw.* **3**, 821. doi:10.21105/joss.00821

Schlegel, R. W., Oliver, E. C. J., Wernberg, T. and Smit, A. J. (2017). Nearshore and offshore co-occurrence of marine heatwaves and cold-spells. *Prog. Oceanogr.* **151**, 189-205. doi:10.1016/j.pocean.2017.01.004

Schunter, C., Jarrold, M. D., Munday, P. L. and Ravasi, T. (2021). Diel pCO_2 fluctuations alter the molecular response of coral reef fishes to ocean acidification conditions. *Mol. Ecol.* **30**, 5105-5118. doi:10.1111/mec.16124

Schwemmer, T. G., Baumann, H., Murray, C. S., Molina, A. I. and Nye, J. A. (2020). Acidification and hypoxia interactively affect metabolism in embryos, but not larvae, of the coastal forage fish *Menidia menidia*. *J. Exp. Biol.* **223**, jeb228015. doi:10.1242/jeb.228015

Seebacher, F., White, C. R. and Franklin, C. E. (2015). Physiological plasticity increases resilience of ectothermic animals to climate change. *Nat. Clim. Change* **5**, 61-66. doi:10.1038/nclimate2457

Shannon, L., Coll, M., Neira, S., Cury, P. and Roux, J.-P. (2009). Impacts of fishing and climate change explored using trophic models. In *Climate Change and Small Pelagic Fish* (ed. C. Roy, D. Checkley, J. Alheit and Y. Oozeki), pp. 158-190. Cambridge: Cambridge University Press.

Shelton, A. O., Francis, T. B., Williams, G. D., Feist, B., Stick, K. and Levin, P. S. (2014). Habitat limitation and spatial variation in Pacific herring egg survival. *Mar. Ecol. Prog. Ser.* **514**, 231-245. doi:10.3354/meps10941

Siple, M. C. and Francis, T. B. (2016). Population diversity in Pacific herring of the Puget Sound, USA. *Oecologia* **180**, 111-125. doi:10.1007/s00442-015-3439-7

Siple, M. C., Shelton, A. O., Francis, T. B., Lowry, D., Lindquist, A. P. and Essington, T. E. (2017). Contributions of adult mortality to declines of Puget Sound Pacific herring. *ICES J. Mar. Sci.* **75**, 319-329. doi:10.1093/icesjms/fsx094

Small, M. P., Loxterman, J. L., Frye, A. E., Von Bargen, J. F., Bowman, C. and Young, S. F. (2005). Temporal and spatial genetic structure among some pacific herring populations in Puget Sound and the Southern Strait of Georgia. *Trans. Am. Fish. Soc.* **134**, 1329-1341. doi:10.1577/T05-050.1

Sswat, M., Stiasny, M. H., Jutfelt, F., Riebesell, U. and Clemmesen, C. (2018). Growth performance and survival of larval Atlantic herring, under the combined effects of elevated temperatures and CO_2. *PLoS ONE* **13**, e0191947. doi:10.1371/journal.pone.0191947

Szuwalski, C. S. and Hilborn, R. (2015). Environment drives forage fish productivity. *Proc. Natl Acad. Sci. USA* **112**, E3314-E3315. doi:10.1073/pnas.1507990112

Szuwalski, C. S., Britten, G. L., Licandeo, R., Amoroso, R. O., Hilborn, R. and Walters, C. (2019). Global forage fish recruitment dynamics: a comparison of methods, time-variation, and reverse causality. *Fish. Res.* **214**, 56-64. doi:10.1016/j.fishres.2019.01.007

Tabachnick, B. G., Fidell, L. S. and Ullman, J. B. (2007). *Using Multivariate Statistics*. Boston, MA: Pearson.

Takle, H., Baeverfjord, G., Lunde, M., Kolstad, K. and Andersen, Ø. (2005). The effect of heat and cold exposure on HSP70 expression and development of deformities during embryogenesis of Atlantic salmon (*Salmo salar*). *Aquaculture* **249**, 515-524. doi:10.1016/j.aquaculture.2005.04.043

Talbot, K., Kwong, R. W. M., Gilmour, K. M. and Perry, S. F. (2015). The water channel aquaporin-1a1 facilitates movement of CO_2 and ammonia in zebrafish (*Danio rerio*) larvae. *J. Exp. Biol.* **218**, 3931-3940. doi:10.1242/jeb.129759

Thomsen, M. S., Mondardini, L., Alestra, T., Gerrity, S., Tait, L., South, P. M., Lilley, S. A. and Schiel, D. R. (2019). Local extinction of bull kelp (*Durvillaea* spp.) due to a marine heatwave. *Front. Mar. Sci.* **6**, 00084. doi:10.3389/fmars.2019.00084

Tiedke, J., Cubuk, C. and Burmester, T. (2013). Environmental acidification triggers oxidative stress and enhances globin expression in zebrafish gills. *Biochem. Biophys. Res. Commun.* **441**, 624-629. doi:10.1016/j.bbrc.2013.10.104

Tomasetti, S. J., Kraemer, J. R., , Jr and Gobler, C. J. (2021). Brief episodes of nocturnal hypoxia and acidification reduce survival of economically important blue crab (*Callinectes sapidus*) larvae. *Front. Mar. Sci.* **8**, 720175. doi:10.3389/fmars.2021.720175

Tseng, Y.-C., Hu, M. Y., Stumpp, M., Lin, L.-Y., Melzner, F. and Hwang, P.-P. (2013). CO$_2$-driven seawater acidification differentially affects development and molecular plasticity along life history of fish (*Oryzias latipes*). *Comp. Biochem. Physiol. A Mol. Integr. Physiol.* **165**, 119-130. doi:10.1016/j.cbpa.2013.02.005

Villalobos, C., Love, B. A. and Olson, M. B. (2020). Ocean acidification and ocean warming effects on Pacific herring (*Clupea pallasi*) early life stages. *Front. Mar. Sci.* **7**, 597899. doi:10.3389/fmars.2020.597899

von Biela, V. R., Arimitsu, M. L., Piatt, J. F., Heflin, B., Schoen, S. K., Trowbridge, J. L. and Clawson, C. M. (2019). Extreme reduction in nutritional value of a key forage fish during the Pacific marine heatwave of 2014-2016. *Mar. Ecol. Prog. Ser.* **613**, 171-182. doi:10.3354/meps12891

Wernberg, T., Smale, D. A., Tuya, F., Thomsen, M. S., Langlois, T. J., de Bettignies, T., Bennett, S. and Rousseaux, C. S. (2013). An extreme climatic event alters marine ecosystem structure in a global biodiversity hotspot. *Nat. Clim. Change* **3**, 78-82. doi:10.1038/nclimate1627

Wetz, M. S. and Yoskowitz, D. W. (2013). An 'extreme' future for estuaries? Effects of extreme climatic events on estuarine water quality and ecology. *Mar. Pollut. Bull.* **69**, 7-18. doi:10.1016/j.marpolbul.2013.01.020

Wickham, H. (2016). *ggplot2: Elegant Graphics for Data Analysis*. New York: Springer-Verlag.

Zhang, Z., Falter, J., Lowe, R., Ivey, G. and McCulloch, M. (2013). Atmospheric forcing intensifies the effects of regional ocean warming on reef-scale temperature anomalies during a coral bleaching event. *J. Geophys. Res. Oceans* **118**, 4600-4616. doi:10.1002/jgrc.20338

Supplementary Materials & Methods.

Heatwave Analysis

Methods: Heatwave dynamics (i.e., duration, rate of onset, and maximum intensity) were determined by analyzing an 18-year temperature dataset (2002-2020) from the NERRS Ploeg Channel monitoring station in Padilla Bay, WA (48°33'22.8"N 122°31'51.2"W). The station code is PDBBPWQ and the dataset was downloaded from the NERRS Centralized Data Management Office (https://cdmo.baruch.sc.edu/dges/). The R package heatwaveR (Schlegel and Smit, 2018) was used to identify heatwaves in the timeseries based on a selection criteria of daily mean temperatures exceeding the 90th percentile of the long-term seasonal climatology for a minimum of 5 consecutive days (Hobday et al., 2016).

Results: A total of 45 events were detected in the 18-year dataset. Heatwaves occurred during all months at a roughly equal frequency between seasons (11 or 12 per season). Maximum intensity ranged from 1.67° - 5.33°C above seasonal climatology, with a mean (±SD) of 2.97±0.79°C. However, there was a clear seasonal fluctuation in maximum heatwave intensity as the strongest events occurred in late-spring and summer. The most extreme event occurred in June 2014. It reached a maximum intensity of 5.32°C with a rate of onset of 0.56 °C×d-1 and lasted for eight consecutive days (Table S1). Event duration ranged from 5 to 20 d (mean 7.3±3.1 d) while rate of onset ranged between 0.08° C × d-1 to 1.01°C × d-1 (mean 0.46±0.22°C × d-1). There was a weak relationship between maximum intensity and rate of onset. More intense heatwaves tended to manifest more quickly, but there were several outlying events (linear regression, p = 0.00289, $r2 = 0.1696$). There was no relationship between maximum intensity and event duration. However, there was a weak negative relationship between rate of onset and duration, such that heatwaves that manifested quickly had shorter durations (linear regression, p = 0.0087, $r2 = 0.1297$). Again, there were clear outlying events to this trend. The period around the 2014-2016 North Pacific Heatwave produced more heatwaves and the most intense events compared to any other period in the timeseries (2014: 7 events, 2015: 12 events, 2016: 7 events, Fig. S1). Most other years experienced just 1-2 events, but a smaller heatwave outbreak occurred during 2003-2005 with 3 – 4 events per year (Fig. S1). Detailed characteristics of the top 10 heatwave events are listed in Table S1.

Converting pH$_{NIST}$ to pH$_T$

Methods: To reduce the error associated with seawater pH measurements calibrated on the NIST scale (Dickson et al., 2015), an extensive cross-calibration was made between the handheld Orion electrode and the diode array spectrophotometer to produce a robust probe-specific linear relationship to convert pH$_{NIST}$ values measured with the handheld to pH$_T$. A total of 36 seawater sample will prepared by stripping or adding small amounts of dissolved CO_2 to seawater to achieve pH levels across the range of pH values recorded during the experiment. All measurements were made room temperature (20-23°C) and a salinity of 32. After vigorously mixing the seawater samples, pH$_{NIST}$ was recorded with the handheld electrode and then the sample was immediately injected into the jacketed cuvette and pHT was measured with the diode array spectrophotometer (Love et al., 2017). A conversion formula was derived by fitting the relationship with a linear model (pHT = 0.91344 × pHNIST + 0.59905, R^2 > 0.99)

Table S1. Summary of the top 10 heatwave events detected at the Ploeg Channel Monitoring Station in Padilla Bay, WA from 2002-2020. Cumulative intensity is sum of daily positive temperature anomaly for the duration of the heatwave.

Rank	Duration (days)	Start	Peak	Max intensity (°C)	Cum. Intensity (°C)	Rate of onset (°C d^{-1})
1	8	6/3/2014	6/8/2014	5.32	30.82	0.56
2	5	4/19/2016	4/22/2016	4.71	17.21	0.67
3	6	6/8/2015	6/11/2015	4.64	21.24	0.65
4	10	6/23/2015	6/26/2015	4.03	34.24	0.33
5	7	7/20/2003	7/23/2003	4.01	18.86	0.61
6	6	7/23/2004	7/25/2004	3.96	16.74	0.79
7	6	5/26/2015	5/30/2015	3.93	18.58	0.53
8	5	4/30/2016	5/3/2016	3.87	13.33	0.57
9	6	7/31/2014	8/4/2014	3.78	16.18	0.54
10	13	3/30/2016	4/1/2016	3.56	32.16	0.84
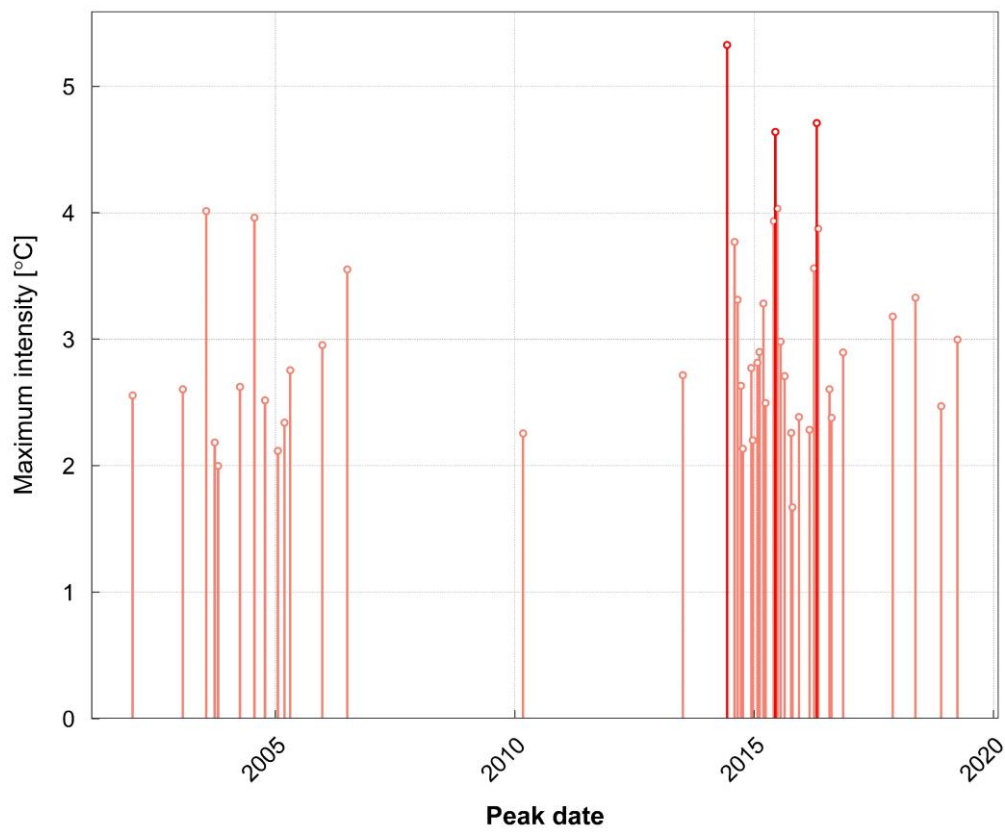
Fig. S1. A lolli-plot of all detected heatwave events. The vertical red lines denote the maximum intensity (°C) of each event.

References

Dickson, A. G., Camões, M. F., Spitzer, P., Fisicaro, P., Stoica, D., Pawlowicz, R. and Feistel, R. (2015). Metrological challenges for measurements of key climatological observables. Part 3: seawater pH. *Metrologia* **53**, R26-R39.

Hobday, A. J., Alexander, L. V., Perkins, S. E., Smale, D. A., Straub, S. C., Oliver, E. C. J., Benthuysen, J. A., Burrows, M. T., Donat, M. G., Feng, M. et al. (2016). A hierarchical approach to defining marine heatwaves. *Progress in Oceanography* **141**, 227-238.

Love, B. A., Olson, M. B. and Wuori, T. (2017). Technical Note: A minimally invasive experimental system for pCO2 manipulation in plankton cultures using passive gas exchange (atmospheric carbon control simulator). *Biogeosciences* **14**, 2675-2684.

Schlegel, R. and Smit, A. (2018). heatwaveR: A central algorithm for the detection of heatwaves and cold-spells. *Journal of Open Source Software* **3**, 821.

Table S2. Pearson correlation coefficients matrix of treatment conditions, morphometric traits, and PC 1-4 scores. Traits are abbreviated as standard length (SL), somatic body area (SBA), head width (HW), eye width (EW), post-yolk body depth (PYBD), post-vent body depth (PVBD), yolk-sac area (YSA), and dry weight (DW).

|	Temp	pCO$_2$	SL	SBA	HW	EW	PYBD	PVBD	YSA	DW	PC1	PC2	PC3	PC4
Temp	-	-	-0.628	-0.461	-0.135	-0.431	-0.16	-0.454	-0.472	-0.177	-0.482	0.004	-0.478	0.065
pCO$_2$	-	-	-0.086	-0.146	-0.148	-0.166	-0.121	-0.174	0.194	0.144	-0.101	0.327	0.076	-0.014
SL	-0.628	-0.086	-	0.906	0.536	0.608	0.487	0.725	0.463	0.403	0.858	-0.134	0.309	-0.224
SBA	-0.461	-0.146	0.906	-	0.733	0.626	0.72	0.81	0.435	0.431	0.948	-0.181	0.001	-0.161
HW	-0.135	-0.148	0.536	0.733	-	0.481	0.687	0.55	0.359	0.322	0.776	-0.139	-0.435	0.201
EW	-0.431	-0.166	0.608	0.626	0.481	-	0.403	0.567	0.332	0.207	0.697	-0.293	0.374	0.497
PYBD	-0.16	-0.121	0.487	0.72	0.687	0.403	-	0.574	0.436	0.412	0.778	0.022	-0.501	0.042
PVBD	-0.454	-0.174	0.725	0.81	0.55	0.567	0.574	-	0.315	0.305	0.816	-0.287	0.099	-0.285
YSA	-0.472	0.194	0.463	0.435	0.359	0.332	0.436	0.315	-	0.679	0.621	0.652	0.147	0.181
DW	-0.177	0.144	0.403	0.431	0.322	0.207	0.412	0.305	0.679	-	0.576	0.714	0.048	-0.122
PC1	-0.482	-0.101	0.858	0.948	0.776	0.697	0.778	0.816	0.621	0.576	-	-	-	-
PC2	0.004	0.327	-0.134	-0.181	-0.139	-0.293	0.022	-0.287	0.652	0.714	-	-	-	-
PC3	-0.478	0.076	0.309	0.001	-0.435	0.374	-0.501	0.099	0.147	0.048	-	-	-	-
PC4	0.065	-0.014	-0.224	-0.161	0.201	0.497	0.042	-0.285	0.181	-0.122	-	-	-	-

Table S3. Summary statistics for LMMs and ANOVAs testing growth traits. Results for LMMs testing individual PC scores and morphometric traits. Numerator degrees of freedom (NumDF) and denomination degrees of freedom (DenDF) are presented. ANOVA results are given for yolk consumption rate (YCR), embryo growth rate (GR), and production efficiency (PE). Significant test results are denoted in bold.

LMMs					
Trait	**Factor**	**NumDF**	**DenDF**	***F***	***p***
PC1	pCO$_2$	1	12	1.347	0.268
	Temp	1	12	22.709	**<0.001**
	pCO$_2$ × temp	1	12	0.212	0.654
PC2	pCO$_2$	1	12	10.270	**0.008**
	Temp	1	12	0.424	0.527
	pCO$_2$ × temp	1	12	1.919	0.191
PC3	pCO$_2$	1	12	0.452	0.514
	Temp	1	12	17.423	**0.001**
	pCO$_2$ × temp	1	12	0.907	0.360
PC4	pCO$_2$	1	12	0.017	0.898
	Temp	1	12	0.362	0.559
	pCO$_2$ × temp	1	12	0.125	0.730
SL	pCO$_2$	1	12	3.442	0.088
	Temp	1	12	54.230	**<0.001**
	pCO$_2$ × temp	1	12	0.037	0.851
SBA	pCO$_2$	1	12	3.313	0.094
	Temp	1	12	21.062	**<0.001**
	pCO$_2$ × temp	1	12	0.001	0.987
HW	pCO$_2$	1	12	1.269	0.282
	Temp	1	12	1.401	0.259
	pCO$_2$ × temp	1	12	0.751	0.403
EW	pCO$_2$	1	12	3.422	0.089
	Temp	1	12	22.948	**<0.001**
	pCO$_2$ × temp	1	12	1.238	0.288
PYBD	pCO$_2$	1	12	0.945	0.350
	Temp	1	12	1.646	0.224
	pCO$_2$ × temp	1	12	0.180	0.679
PVBD	pCO$_2$	1	12	5.599	**0.036**
	Temp	1	12	38.016	**<0.001**
	pCO$_2$ × temp	1	12	0.004	0.952
YSA	pCO$_2$	1	12	3.552	0.084
	Temp	1	12	20.8990	**<0.001**
	pCO$_2$ × temp	1	12	2.071	0.176
DW	pCO$_2$	1	12	1.191	0.297
	Temp	1	12	1.803	0.204
	pCO$_2$ × temp	1	12	1.091	0.317

ANOVAs				
Trait	**Factor**	**DF**	**F**	***p***
YCR	pCO$_2$	1	0.556	0.133
	Temp	1	70.500	**<0.0001**
	pCO$_2$ × temp	1	0.102	0.653
GR	pCO$_2$	1	0.984	0.341
	Temp	1	131.732	**<0.0001**
	pCO$_2$ × temp	1	0.016	0.902
PE	pCO$_2$	1	0.018	0.896
	Temp	1	8.761	**0.012**
	pCO$_2$ × temp	1	0.028	0869
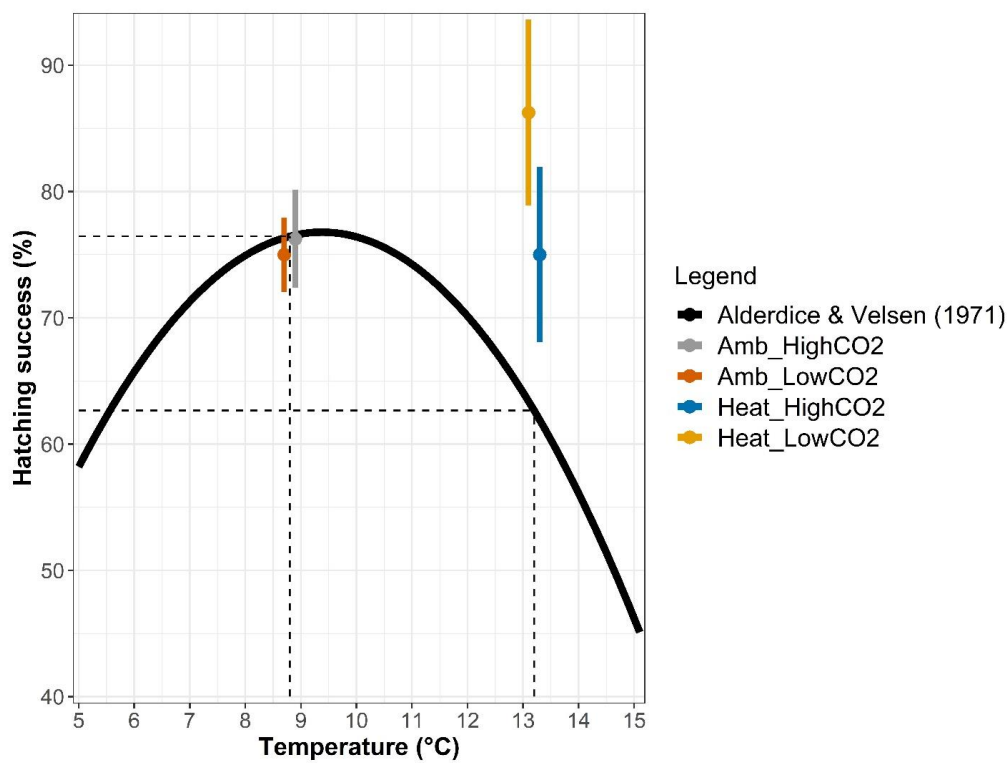
Fig. S2. The thermal reaction norm for embryo survival in Pacific herring. Colored circles denote the average hatching success ± s.d. under the four treatment conditions tested in this study. The solid black curve shows the temperature reaction norm for embryo survival (%) under static temperatures predicted by Alderdice & Velsen (1971) at salinity of 32. Dashed lines connect the predicted survival rates for the ambient temperature regime (~8.8°C) and maximum heatwave intensity (~13.2°C).
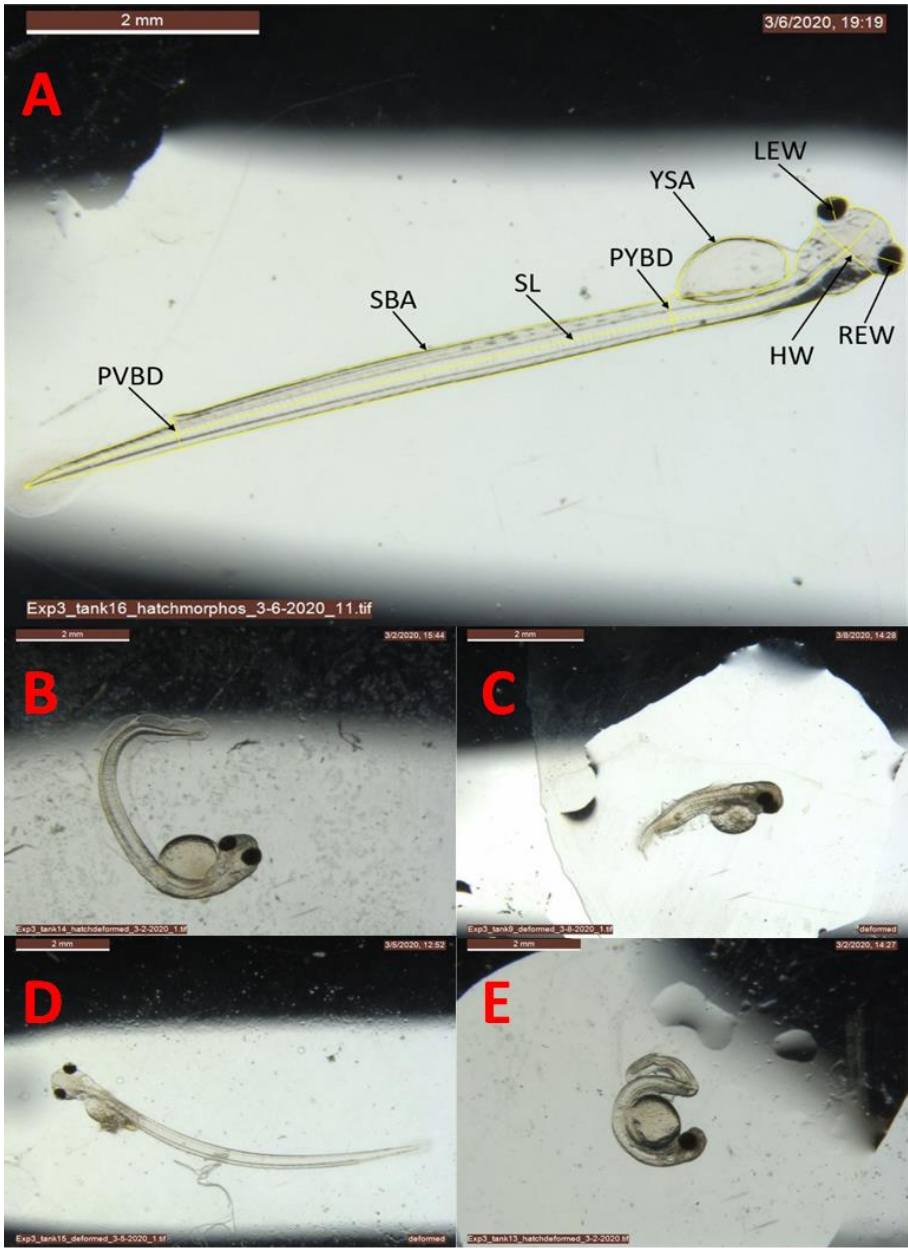
Fig. S3. A. Schematic of the eight morphometric measurements made on healthy hatchings; PVBD (post-vent body depth), SBA (somatic body area), SL (standard length), PYBD (post-yolk body depth), YSA (yolk sac area), HW (head width), LEW (left eye width), REW (right eye width). **B.** Developmental anomaly: notochord curvature **C.** Developmental anomaly: notochord shortening and underdeveloped jaw. **D.** Developmental anomaly: yolk sac edema. **E.** Developmental anomaly: notochord twist and underdeveloped jaw.